Chapter - 8

In-vitro Characterization of PEGylated Liposomes & Immunoliposomes

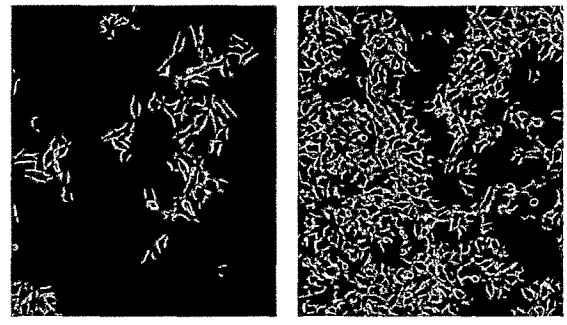

8.1. Morphology study

The morphology of prepared PEGylated multilamellar vesicles (MLVs) was studied by optical microscopy and single unilamellar vesicles (SUVs) (formed after probe sonication) by transmission electron microscopy.

8.1.1. Olympus microscopy

Morphological evaluation was conducted using optical microscope with polarizer BX 40, Olympus Optical Co. Ltd., at a magnification of 40X. A drop of liposome was placed on glass slide, covered with coverslip, observed under optical microscope and images were captured.

8.1.2. Transmission electron microscope (TEM)

Morphology and size of the liposomal suspension was studied by transmission electron microscope (TEM). A drop of formulation was placed on a coated carbon grid and air dried. The samples were stained with 5µL of 2.5 % uranyl acetate for 30 seconds and air dried. The grid was then examined immediately under Philips Electron Microscope (Philips, Japan). The electron micrographs were obtained after magnifications. The physical characteristics of the particles observed by TEM were determined using selected area diffraction (SAD) technique. The measurement conditions were $\lambda = 0.0251$ A^0 radiation generated at 200kV as X-ray source with camera length of 100cm.

8.2. FTIR Study

The plain docetaxel, freeze-dried docetaxel loaded PEGylated liposomes and blank PEGylated liposomes were analysed using FT-IR Alpha-T (Bruker, Germany).

8.3. Differential scanning calorimetry (DSC)

Thermal properties of plain docetaxel, physical mixture of docetaxel and other lipids (HSPC, DPPC, cholesterol, and DSPE-mPEG$_{2000}$, 50:50 w/w), and freeze dried docetaxel loaded PEGylated liposomes were investigated using Differential Scanning Calorimetry (METTLER, STAR^e SW 9.20). Accurately weighed samples (7.2-11.5mg) were placed in hermetically closed aluminum pans and empty aluminum pan was used as a reference. The samples were heated at a heating rate of 100 ^{0}C per minute in the range of -50 ^{0}C to 250 ^{0}C under inert nitrogen atmosphere.

8.4. Controlled drug release

Release of docetaxel from PEGylated liposomes (PLs) and immunoliposomes (PILs) was observed using the dialysis method and was compared Taxotere (Sanofi Aventis). The release of DTX from PLs composed of HSPC alone and DPPC alone was also studied. The Taxotere, PLs and PILs equivalent to 1mg of docetaxel were placed in dialysis tubes (MWCO 12000) and tightly sealed. Then, the tubes were immersed in 50mL of release medium, *i.e.*, PBS (pH 7.4) containing 0.1% (w/v) tween-80 to maintain sink condition (Koziara et al., 2004; Zhang et al., 2004; Yang et al., 2007). While stirring the release medium using the magnetic stirrer at 150 rpm/min, the samples (1mL) were withdrawn

at predetermined time intervals (0.5, 1, 2, 4, 6, 10, 24, 48hr) from the release medium and the same volume was replaced with the fresh medium. The 1mL of sample was centrifuged at 5000 rpm for 5 minutes and the supernatant was bath sonicated for 5 minutes and analysed using RP-HPLC (as described in analytical method) using acetonitrile:water (60:40, v/v) as mobile phase. The concentration of docetaxel released with respect to time was then calculated. The concentration of docetaxel remained unreleased in dialysis bag was calculated by dissolving dialysis bag contents in methanol after the release study to check the mass balance. The samples were centrifuged, supernatant was sonicated, and analysed using RP-HPLC. The stability of DTX in release medium was also studied by determining the amount of DTX impurities converted in release medium at each time point.

8.5. Suspension stability study

The liposomal suspension stability study was performed as per the ICH guidelines at 2-8 ^{0}C for 6 months. The stability of PEGylated liposomes in the absence and presence of 10% sucrose (used as tonicity adjusting agent) was studied. 1mL of the PEGylated liposomal formulations (n=4) were stored in nitrogen purged screw capped glass vials at 2-8 ^{0}C for a period of 6 months. After 1, 2, 4, and 6 months the formulations were transferred to 2mL eppendorf tubes and centrifuged at 6000rpm for 10 minutes. The supernatant liposomal dispersion was separated from the sediment (containing leaked drug) and analysed for mean particle size, zeta potential and % DTX retained. The liposomal suspensions were also evaluated for degradation of DTX during storage (stability of DTX in liposomes during storage).

8.6. *In vitro* cytotoxicity assay

The cytotoxicity of Taxotere and docetaxel loaded conventional liposomes (CLs), PLs and PILs against A549 (human lung adenocarcinoma) and B16F10 (mouse melanoma) cell line was determined using MTT dye reduction assay (Twentyman and Luscombe, 1987). Briefly, 4×10^{3}, 2×10^{3}, and 1.5×10^{3} cells in exponential phase were seeded into 96-well plates for 24hr, 48hr, and 72hr, respectively. The cells were incubated at 37 ^{0}C in a 5% CO_2 incubator for 24hr, during which the cells were attached and resumed to grow. The formulations were diluted with culture media to make serial concentrations of docetaxel (0.01nM, 0.1nM, 1nM, 10nM, 100nM, 1μM, 10μM), and were added to wells in quadruplicate (100μL each). Control wells were treated with equivalent volumes of docetaxel-free media. After 24h, 48h, and 72h, the supernatant was removed and each well was washed twice with 100μL of PBS. The 20μL of MTT (5mg/mL solution in PBS pH 7.4) and 80μL of culture medium were added to each well and incubated for overnight. The plates were then centrifuged for 20 minutes at 1500rpm (Rota 4R-V/F_M; Plasters Crafts Industries Ltd., Mumbai, India) and the unreduced MTT and medium were then discarded. The 100μL of DMSO was then added to dissolve the MTT formazan crystals. Plates were shaken for 2min and absorbance was read at dual wavelengths of 540/690nm as excitation and reference using the microplate reader (Molecular Devises,

SPECTRUM AX190). The IC_{50} values were then calculated graphically (logarithmic scale) by plotting concentrations versus % viability. The % viability was calculated by considering the optical density of the control well as 100% viable (Sharma et al., 1996).

8.7. Cell uptake study

8.7.1. Preparation of 6-coumarin loaded liposomes

The 6-coumarin loaded CLs, PLs, and PILs were prepared as described in previous chapters by just replacing DTX from 100µg of 6-coumarin. The lipid concentrations and other process and formulation parameters were kept similar to the preparation of optimized DTX loaded CLs, PLs and PILs. The total lipid concentration of prepared liposomes was determined by Stewart method as described in previous chapters. The prepared 6-coumarin loaded liposomes were stored in amber coloured vials, covered with aluminium foil, at 2-8 ^{0}C.

8.7.2. Cell uptake study using FACS

The 2 million cells per well were transferred to 12 well plate and then were allowed to adhere and grow overnight. The cells were treated with 1mL of media containing 6-coumarin loaded CLs, PLs and PILs equivalent to 25µg and 50µg of total lipid content for 30 and 60 minutes. Cells were washed thrice with PBS and harvested. The cells were then fixed using 1% PFA for 10 minutes and then washed twice with PBS. Acquisition was done using FACS Calibur.

8.7.3. Cell uptake study using confocal microscopy

The cells were grown on glass coverslips up to 50-60% confluency and then were treated with CLs, PLs and ILs equivalent to 25µg and 50µg of total lipid content for period of 30 and 60 minutes. Cells were washed thrice with PBS and then fixed using 1% PFA. Coverslips were washed again with PBS, mounted and visualized under confocal microscope Zeiss LSM 510 Meta at 63 X magnification.

8.7.4. Live cell uptake imaging by confocal microscope

5×10^4 A549 cells were allowed to adhere and grow in live imaging culture plates overnight. 200µl of 6-coumarin loaded CLs, PLs, and PILs (25µg of total lipid/mL) were added just prior to time lapse imaging. Live imaging was performed using confocal microscope (LSM 510 Meta) at 63X magnification at regular intervals of 30 seconds. The cells were maintained at 37 ^{0}C and supplied with 5% CO_2 during the imaging as per earlier reports (Pollock et al., 2010; Xie et al., 2012). Images were analysed by LSM image browser software and were digitalised to video format.

8.8. Anti-metastatic activity by wound scratch assay

The wound healing assay was performed as per the earlier reports (Goel and Gude 2011; Pichot et al., 2009; Lee et al., 2008). Cells grown in 12-well plates were treated with 1µg/ml mitomycin-C for 2hr. The cells were then lined off using a sterile tip, and the wells were washed to ensure that the wound area is devoid of cells. The 2mL of sub-

toxic doses (1nM and 2nM) of DTX, PLs, and PILs were added and incubated at 37 ^{0}C in a 5% CO_2 incubator for 24hr. The drug solution was removed, cells were washed twice with PBS, fixed using 70% methanol and photographed using Axiovert200 inverted microscope (Zeiss). The reference well cells were fixed immediately after wound was made and the control well cells were incubated with 2mL of drug free media. The wound width was measured using the Carl Zeiss Axiovision Rel 4.8.2 imaging software and the results were presented as percent wound covered by considering the control group width as 100% wound covered.

8.9. Gelatin zymography

8.9.1. Introduction

Matrix metalloproteinases (MMPs) are a family of calcium-dependent, zinc-containing endopeptidases that are structurally and functionally related. They are secreted in an inactive (latent) form, which is called a zymogen or a pro-MMP. These latent MMPs require an activation step before they are able to cleave extracellular matrix (ECM) components (Bode and Maskos, 2003). The activity of MMPs is regulated by several types of inhibitors, of which the tissue inhibitors of metalloproteinases (TIMPs) are the most important (Brew et al., 2000). The TIMPs are also secreted proteins, but they may be located at the cell surface in association with membrane-bound MMPs (Baker et al., 2002). The balance between MMPs and TIMPs is largely responsible for the control of degradation of ECM proteins (Bode et al., 1999). MMPs are involved in the remodeling of tissues during embryonic development, cell migration, wound healing, and tooth development (Pilcher et al., 1999; Chin and Werb, 1997). However, a deregulation of the balance between MMPs and TIMPs is a characteristic of diverse pathological conditions, such as rheumatoid and osteoarthritis, cancer progression, and acute and chronic cardiovascular diseases (Baker et al., 2002; Konttinen et al., 1999). To analyze the role of MMPs and TIMPs in tissue remodeling under normal and pathological conditions, it is important to have reliable detection methods.

Substrate Zymography:

Zymography and reverse zymography are described as simple, sensitive, quantifiable, and functional assays to analyze MMPs and TIMPs in biological samples (Leber et al., 1997). All types of substrate zymography originate from gelatin zymography. The techniques are the same except that the substrate differs depending on the type of MMPs or TIMPs to be detected. In zymography, the proteins are separated by electrophoresis under denaturing [sodium dodecyl sulfate (SDS)], nonreducing conditions. The separation occurs in a polyacrylamide gel containing a specific substrate that is co-polymerized with the acrylamide (Heussen and Dowdle, 1980). During electrophoresis, the SDS causes the MMPs to denature and become inactive. The activation of latent MMPs during zymography is believed to involve the "cysteine switch" because the dissociation of Cys^{73} from the zinc molecule is caused by SDS (Springman et al., 1990). After electrophoresis, the gel is washed, which causes the

exchange of the SDS with Triton X-100, after which the enzymes partially renature and recover their activity (Heussen and Dowdle, 1980). Additionally, the latent MMPs are auto-activated without cleavage (Oliver et al., 1997). Subsequently, the gel is incubated in an appropriate activation buffer. During this incubation, the concentrated, renatured MMPs in the gel will digest the substrate. After incubation, the gel is stained with Coomassie Blue, and the MMPs are detected as clear bands against a blue background of undegraded substrate (Fernandez-Resa et al., 1995). The clear bands in the gel can be quantified by densitometry (Woessner, 1995). Zymography is based on the following principles: (i) during electrophoresis, gelatin is retained in the gel; (ii) MMP activity is reversibly inhibited by SDS during electrophoresis; and (iii) the SDS causes the separation of MMP-TIMP complexes during electrophoresis. This enables the detection of MMPs and TIMPs independently of one another (Hawkes et al., 2001). An additional advantage of zymography is that both the proenzymes and the active forms of MMPs can be distinguished on the basis of their molecular weight. As mentioned before, SDS dissociates the TIMPs from the MMPs, which may result in a higher activity than *in vivo*. Because zymography only indicates whether the proenzyme displays in the presence of TIMP *in vivo*, it is uncertain how much activity such an active form would display in the presence of TIMP *in vivo*. Additionally, the refolding of MMPs after electrophoresis recovers only part of the original activity. Furthermore, the digestion of gelatin by pro-MMPs is somewhat reduced because the latent form still retains its propeptide domain (Woessner, 1995).

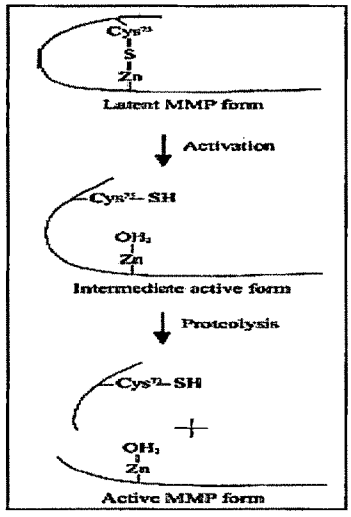

The activation of pro-MMPs. The activation of latent MMPs involves a disruption of the Cys^{73}-Zn^{2+} bond that results in an intermediate active form. During zymography, the latent MMP unfolds due to SDS. The fully active MMP form is formed *in vivo* through proteolysis (Springman et al., 1990).

Gelatin Zymography (Heussen and Dowdle, 1980):

Gelatin zymography is mainly used for the detection of the gelatinases, MMP-2 and MMP-9, respectively. It is extremely sensitive because levels of 10pg of MMP-2 can already be detected (Kleiner and Stetler-Stevenson, 1994). It should be considered, however, that other MMPs, such as MMP-1, MMP-8, and MMP-13 can also lyse the substrate. This signal will probably be very weak because gelatin is not their preferential substrate (Bjornland et al., 1999). For MMPs that do not show any activity on gelatin, modifications of the technique have been made for an improved detection. This is mainly done by incorporating a more suitable substrate into the gel, such as casein or collagen, or by enhancing the signal by adding heparin to the samples (Yu and Woessner, 2001).

Reagents:

Sample Buffer (4X), pH 6.8: 10% SDS, 40% Glycerol, 0.01% Bromophenol blue and 1M Tris HCl.

2% Gelatin: Add 1gm porcine gelatine to 25mL of sterile milliQ water, heat to 70 ^{0}C to dissolve the gelatin and make up the volume to 50mL. Made 2mL aliquots and stored at -20 ^{0}C until use. The 1.5ml of the gelatine solution was added to 30ml of resolving gel mixture during experiment.

Staining solution: 0.5% Coomassie Brilliant Blue R250 powder was dissolved in a destaining solution. Filtered and stored until use.

Destaining solution: methanol, water and acetic acid mixture (4:5:1, v/v).

Other reagents include SDS -PAGE reagents.

8.9.2. Method

Sub-confluent plates (A549) were treated with 3mL of non-toxic doses of TXT (2nM), PLs (2nM), and PILs (2nM) for 24 h. In case of B16F10 the cells were treated with 3mL of nontoxic doses of TXT (5nm), PLs (5nm), and PILs (5nm) for 24hr. The drug solutions were removed and cells were washed twice with PBS to remove serum traces. The 3mL of serum free DMEM was then added to each plate and the condition media was collected after 24hr. The media was concentrated using 30kDa (MWCO) cut-off filters from Millipore and normalised as per the individual cell counts. In addition, the condition medium collected from HT-1080 was also processed and used as a positive control that shows activity of both MMP-9 (92kDa) and MMP-2 (72kDa). To assess the gelatinase activity, the samples (40µL) were incubated in sample buffer for 10 minutes at room temperature and run on 10% SDS-PAGE containing 0.1% gelatin (w/v) as a substrate. After electrophoresis, the gel was washed twice in rinsing buffer (2.5% Triton X-100) for 15 minutes each and then incubated in developing buffer (Tris 50mM, $CaCl_2$ 100mM, $ZnCl_2$ 10µM, Triton X-100 2.5% and NaN_3 0.02%) for at least 24hr. The gel was stained with 0.25% commassie brilliant blue R-250 and then destained (Water: Methanol: Acetic acid; 5:4:1, v/v) till the bands appeared. The gelatinase activity was visible as clear white zones in a dark background. Gel image was taken in the gel

documentation machine and densicord analysis of the band intensity was done (Wang et al., 2009).

8.10. Apoptosis assay

8.10.1. Using FACS

Sub-confluent plates were treated with 1mL of 2nM solution of TXT, PLs and PILs for a period of 24hr and 48hr. Cells were harvested, mixed with supernatant containing apoptic cells, washed twice with PBS and fixed with 70% chilled ethanol. The cells were washed twice with PBS and then incubated with 200µl PBS containing 10µl RNAse (0.5 mg/ml) for 30minutes at 37 ^{0}C. The volume was then made up to 1mL and 50µl PI (50 µg/ml) was added. Acquisition was done on FACS Calibur. The 10000 events were collected and then analysed using CellQuest software (Salma and McDermott, 2012; Kanzawa et al., 2003).

8.10.2. Using EB/AO staining

Ethidium Bromide (EB)/Acridine Orange (AO) staining was done as previously described (Goel and Gude, 2011). 16,000 cells/well were seeded in triplicates in a 96-well plate. The cells were allowed to adhere overnight and then treated with 100µL/well of 2nM of Taxotere, docetaxel loaded PEGylated liposomes and PEGylated anti-neuropilin-1 immunoliposomes for 24hr and 48hr. The cells were then centrifuged and stained using 20µL of EB/AO mixture (100µg/ml) and observed under a Zeiss Axio inverted microscope. Images were captured at X10 magnification for three different fields of each particular well.

8.11. Cell cycle analysis

The protocol is same as discussed in apoptosis study. The 10000 events were collected and analysed for cell cycle using ModFit LT V2.0 (PMac) software.

8.12. Results and Discussions

8.12.1. Morphology analysis

The optical microscopic images of prepared final PEGylated liposomes (MLVs: before probe sonication) were shown in Figure 8.1. The PEGylated liposomes were then probe sonicated to obtain SUVs and analysed using transmission electron microscope (TEM) (Figure 8.2). The optical microscopic and TEM images clearly reveal that the prepared PEGylated liposomes, both MLVs and SUVs, respectively were of spherical in nature.

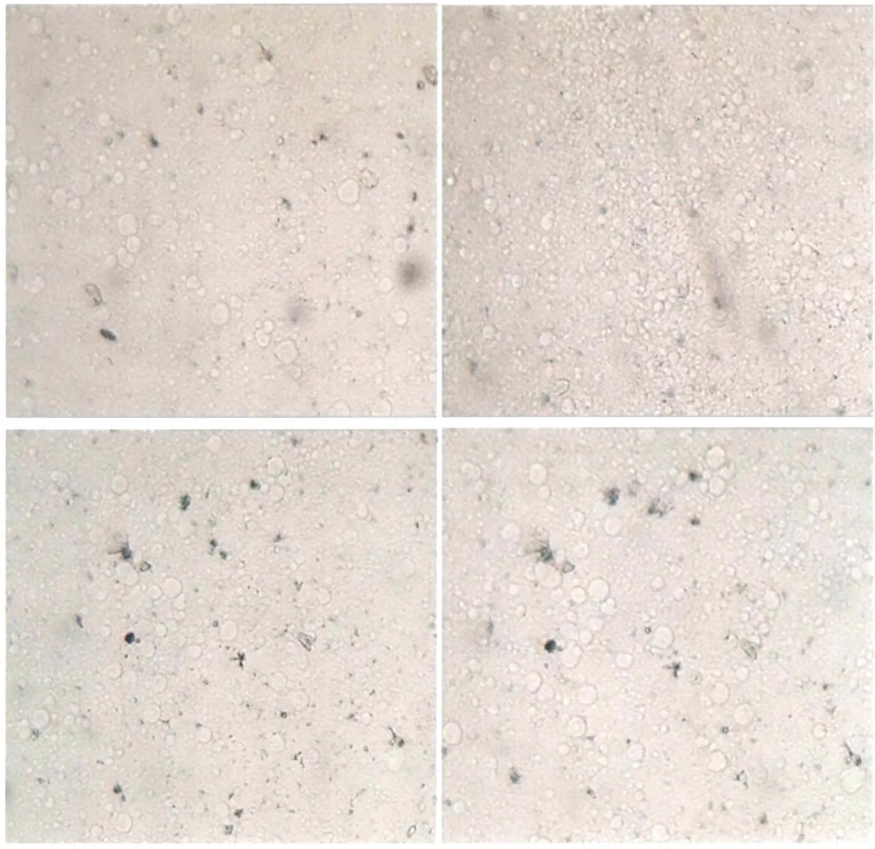

Figure 8.1. Optical microscopic images (10X) of PEGylated liposomes (MLVs: before probe sonication).

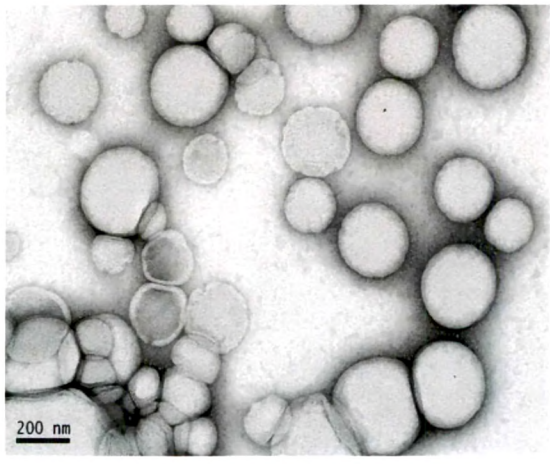

Figure 8.2. Transmission electron microscopic (TEM) images of PEGylated liposomes (SUVs obtained after probe sonication).

8.12.2. FTIR Study

The FTIR spectra of plain docetaxel (Figure 8.3A) showed the carbonyl stretching due to ester group at 1701 cm^{-1}. Further strong band was observed at 1243 cm^{-1} and 1161 cm^{-1} due to C-O stretching. Peak at 706 cm^{-1} indicates presence of mono-substituted aryl groups. The FTIR spectra of docetaxel loaded PEGylated liposomes showed (Figure 8.3B) peaks corresponding to docetaxel functional groups indicating no chemical interaction of docetaxel with other components of the final formulation. Hence, these excipients can be used successfully in the preparation of docetaxel loaded PEGylated liposomes.

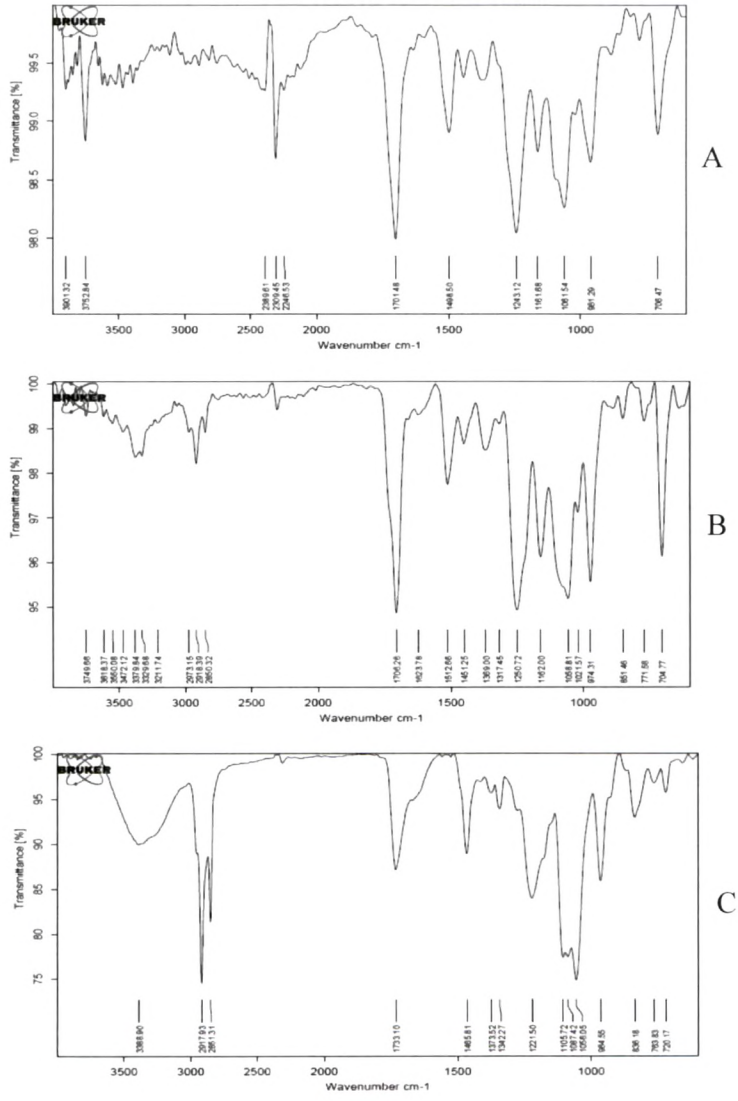

Figure 8.3. The FTIR spectrum of (A) plain docetaxel, (B) docetaxel loaded PEGylated liposomes and (C) blank PEGylated liposomes

8.12.3. Differential scanning calorimetry

DSC analysis was performed for docetaxel (Figure 8.4a), physical mixture of docetaxel and other lipids (Figure 8.4b), and freeze dried docetaxel loaded PEGylated liposomes (Figure 8.4c). The sensitivity of glass transition is directly proportional to sample heating rate and sample mass (Thomas LC, 2001; Lee et al., 2011; Grest and Cohen, 1980). Therefore, in the present study, the DSC analysis was performed at high heating rate of 100 ^{0}C to detect even small amount drug undergone polymorphic changes. The DSC thermogram of plain docetaxel showed little broad peak corresponding to docetaxel in the range of 180-188 °C. The DSC thermogram of plain docetaxel also showed a peak at 115.8 ^{0}C corresponds to loss of residual water from docetaxel. In the DSC thermogram of physical mixture we observed a peak corresponding to docetaxel at 187.7 ^{0}C. This melting peak was absent in the DSC thermogram of docetaxel loaded PEGylated liposomes indicates the docetaxel present in amorphous form and in molecular state after entrapped into the liposomal bilayer. The DSC thermogram of physical mixture also showed two endothermic peaks one at 81.4 ^{0}C and second at 130.9 ^{0}C and these peaks might correspond to lipid mixture. The similar peaks were also observed in docetaxel loaded PEGylated liposomes (one at 66 ^{0}C and second at 137 ^{0}C).

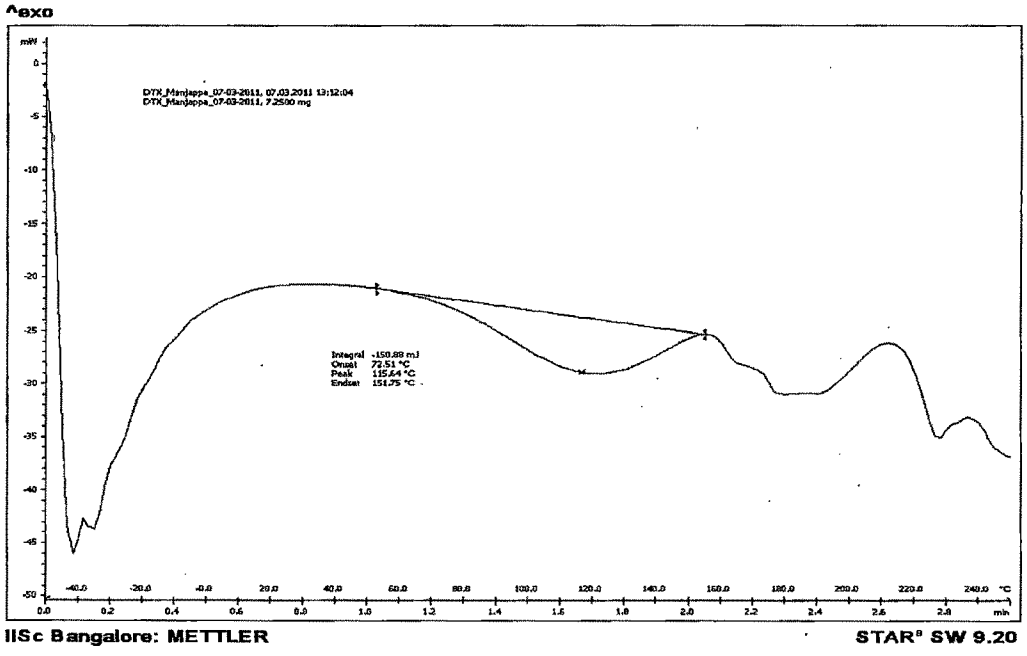

Figure 8.4(a). DSC thermogram of plain docetaxel

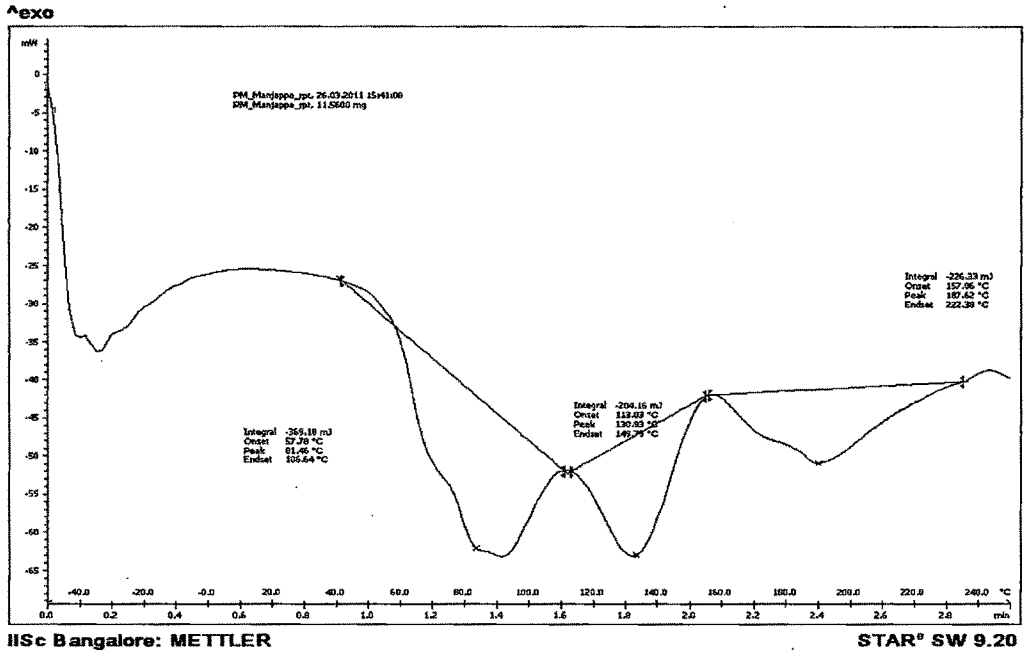

Figure 8.4(b). DSC thermogram of physical mixture of docetaxel and other components of PEGylated liposomes (HSPC, DPPC, Cholesterol, and DSPE-mPEG$_{2000}$, 50:50 w/w)

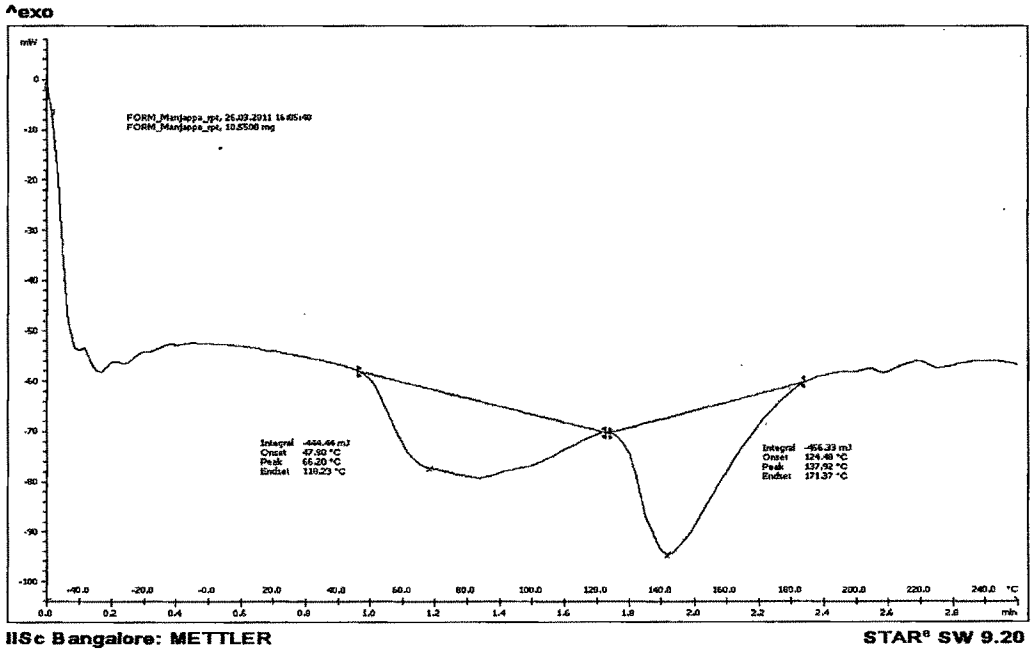

Figure 8.4(c). DSC thermogram of docetaxel loaded PEGylated liposomes

8.12.4. Controlled drug release

The 0.1% (w/v) of tween-80 was added in the release medium (PBS, pH 7.4) to maintain sink condition during the release study. The *in vitro* controlled drug release from Taxotere, PEGylated liposomes composed of HSPC alone, DPPC alone and HSPC:DPPC (1:1) were studied and results are represented in Table 8.1 and Figure 8.5. The drug release was better controlled in all PEGylated liposomal formulations as compared to marketed Taxotere (49.957±4.22%) after 48hr of release study. The liposomal formulation composed of both HSPC:DPPC showed better control of DTX release (19.898±0.507%) as compared to PEGylated liposomes composed of HSPC alone (31.976±1.503%) and DPPC alone (26.454±0.341%) after 48hr of release study. The controlled release of DTX from PEGylated liposomes composed of HSPC:DPPC could be due to altered membrane stability of these liposomes as compared to individual lipids and thus showing depot effect. From the above results it is very clear that the PEGylated liposomes (HSPC:DPPC) releases DTX very slowly in the blood and thereby carrying more DTX to tumor tissues. This indicates PEGylated liposomal formulation composed of HSPC:DPPC has potential as an effective drug delivery system (Song et al., 2006).

The comparison of % DTX release from Taxotere, PLs and PILs was shown in Table 8.2 and Figure 8.6. The PILs showed still better control of DTX release (16.978±0.707%) as compared to Taxotere (49.957±4.223%) and PLs (19.898±0.507%) after 48hr of release study. Therefore, PILs would show much less release of DTX in blood, reach tumour tissue passively and releases the retained drug in the tumor cells upon actively taken *via* neuropilin-1 receptor.

The 7-epidocetaxel is a distinct docetaxel metabolite and Czejka et al. (Czejka et al., 2010) reported, first time, the quantification of 7-epidocetaxel in blood and urine of chemotherapy patients (Taxotere). In 8 of 12 patients 7-epidocetaxel was quantified in plasma at the end of infusion (concentrations ranging from 0.05μg/ml to 0.54μg/ml). In urine, 7-epidocetaxel has been found in 7 of 12 patients (ranged from 3.21μg/ml to 66.37μg/ml). Bornique and Lemarie investigated the interactions of docetaxel and its epimer, 7-epidocetaxel, with recombinant human cytochrome P450 1B1 (hCYP1B1) which is present in various human tumors and is postulated to be responsible for the development of resistance of tumor cells toward chemotherapeutic agents, including docetaxel. The authors observed that at a concentration of 10μM, the 7-epidocetaxel increased the activity of hCYP1B1 by more than 7 fold, confirming that is a potent inducer of this enzyme. Therefore, it is necessary to control the conversion of docetaxel into 7-epidocetaxel in the blood and this can be achieved by better controlling the DTX release from liposomes. The epimerization of released docetaxel into 7-epidocetaxel in the release medium was observed in our study. The more the DTX released from formulation (Taxotere), more will be the formation of 7-epidocetaxel in the release medium (14.06±2.09% after 48hr of study) as compared to other formulations (Table 8.3). The PLs and PILs composed of both HSPC:DPPC showed very less drug release after 48hr study therefore showed less conversion of docetaxel into 7-epidocetaxel

(4.37±0.64% and 3.163±0.48%, respectively). Therefore, the PLs and PILs would better control the DTX release in blood and reaches the maximum amount of active docetaxel, instead of 7-epidocetaxel which helps tumor to develop resistance to docetaxel chemotherapy, to tumor tissue.

Table 8.1. Cumulative % DTX released from different formulations

Time (hr)	Cumulative % DTX released			
	Taxotere	HSPC Alone	DPPC Alone	HSPC:DPPC
0.5	1.66±0.174	1.56±0.037	1.38±0.079	1.24±0.358
1	2.68±0.160	2.01±0.168	1.72±0.351	1.38±1.972
2	3.87±0.616	2.96±0.063	2.98±0.575	2.23±0.144
4	7.42±1.148	4.96±0.196	4.39±0.835	3.98±0.410
6	9.78±2.282	7.44±0.508	6.70±0.605	5.82±0.537
10	18.43±3.289	11.31±0.850	10.79±0.644	9.47±0.831
24	32.83±3.96	20.53±0.58	19.91±0.807	13.27±1.311
48	49.95±4.223	31.97±1.503	26.45±0.341	19.89±0.507

Values are Mean±SD, n=3. The % docetaxel released from all liposomes was found significantly less than marketed Taxotere (***p<0.0001) after 48hr of release study. The % docetaxel released from HSPC:DPPC liposomes was found significantly less than HSPC liposomes (*p<0.05, p=0.001) and DPPC liposomes (*p<0.05, p=0.045) after 48hr of release study.

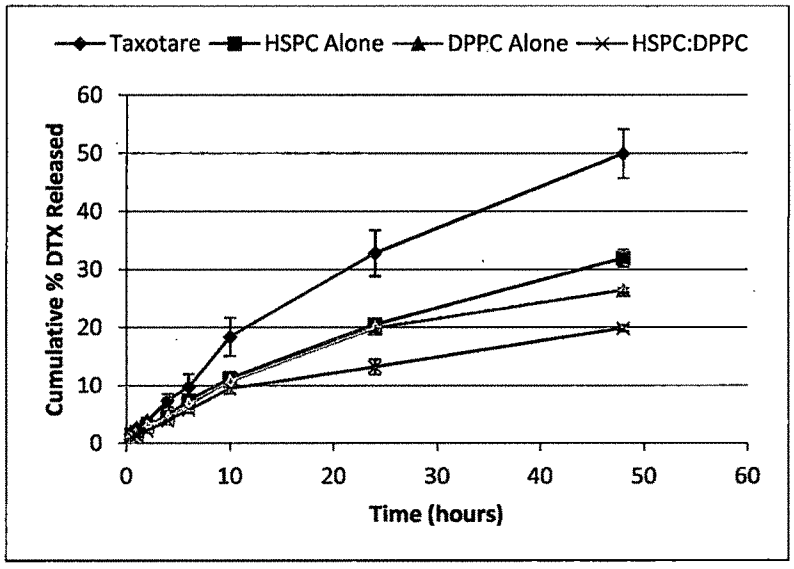

Figure 8.5. Comparison of cumulative % DTX released from different formulations

Table 8.2. Comparison of % cumulative DTX released from PLs and PILs with Taxotere

Time (hr)	Cumulative % DTX released		
	Taxotare®	PLs	PILs
0.5	1.66±0.174	1.24±0.358	0.834±0.458
1	2.68±0.160	1.38±1.972	1.18±0.343
2	3.87±0.616	2.23±0.144	1.95±0.254
4	7.42±1.148	3.98±0.410	2.89±0.576
6	9.78±2.282	5.82±0.537	4.32±0.762
10	18.43±3.289	9.47±0.831	6.29±1.162
24	32.83±3.96	13.27±1.311	10.63±1.221
48	49.95±4.223	19.89±0.507	16.97±0.707

Values are Mean±SD, n=3. PLs: PEGylated liposomes; PILs: PEGylated immunoliposomes

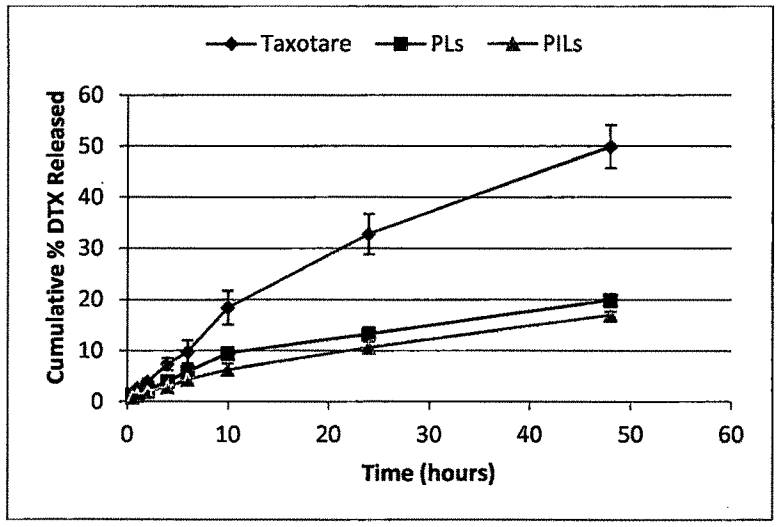

Figure 8.6. Comparison of % cumulative DTX released from PLs and PILs with Taxotere

Table 8.3. Formation of docetaxel impurities in release medium of different formulations

Time (hr)	Taxotere		HSPC Alone		DPPC Alone		HSPC:DPPC	
	%7-EPI	%10-Oxo	%7-EPI	%10-Oxo	%7-EPI	%10-Oxo	%7-EPI	%10-Oxo
10	3.16±0.57	--	0.80±0.10	--	0.793±0.09	--	0.39±0.02	--
24	6.89±1.70	--	3.08±0.22	--	3.43±0.072	0.28±0.084	1.96±0.11	--
48	14.06±2.09	1.95±0.22	7.31±0.39	0.70±0.095	7.85±0.77	0.71±0.079	4.37±0.64	0.27±0.17
Impurities remain unreleased in formulations after 48hr of incubation with PBS (pH 7.4)								
	11.34±3.29	1.254±0.12	4.66±0.18	0.25±0.05	2.81±0.32	0.16±0.11	1.86±0.24	0.13±0.03

7-EPI: 7-Epidocetaxel; 10-Oxo: 10-oxo-7-epidocetaxel. Values are Mean±SD, n=3. The % 7-epidocetaxel formed in release medium was found significantly more with Taxotere as compared to HSPC liposomes (**$p<0.001$), DPPC liposomes (*$p<0.05$, $p=0.00116$), and HSPC:DPPC liposomes (***$p<0.0001$) after 48hrs of release study. The % 7-epidocetaxel formed in the release medium was found significantly less with HSPC:DPPC liposome as compared to DPPC liposomes (*$p<0.05$) after 48hrs of release study. The % 7-epidocetaxel formed and remain unreleased from Taxotere after 48hr of release study was found significantly high as compared to HSPC liposomes (*$p<0.05$), DPPC liposomes (*$p<0.05$) and HSPC:DPPC liposomes (**$p<0.001$).

8.12.5. *In vitro* suspension stability

The PEGylated liposomal suspension stability study results are represented in Table 8.4 and Figure 8.7. The PLs in the presence of 10% sucrose showed better *in vitro* stability than PLs containing no sucrose. The % DTX content of PLs containing sucrose remain unchanged till 4 months but when we analysed after 6th month they showed about 19% decrease in DTX content as compared to PLs containing no sucrose (about 42% decrease in DTX content). Also, the PLs containing no sucrose showed about 20% decrease in DTX content just after one month, the remaining 80% DTX was retained till 4 months. These results indicate that the presence of sucrose in the liposomal formulations (as tonicity adjusting agent) will increase the liposomal suspension stability *in vitro*. This increased stability could be due to increased viscosity of the PLs suspension in the presence of 10% sucrose resulting in decreased particles interactions leading to better retention of loaded DTX content.

The mean particle size (119±6nm; PDI: 0.228±0.04) and zeta potential (-56±2.1mV) of PEGylated liposomes remained unchanged for a period of 4 months irrespective of the presence or absence of sucrose. However, after 6th months of storage, we observed increase in mean particle size (480±20nm; PDI: 0.523±0.129) and decrease in zeta potential (-32±4mV) of PLs suspension containing no sucrose as compared to PLs containing sucrose (188±11nm; PDI: 0.287±0.078; zeta potential: -51±1.4mV). This indicates the need for an increase in viscosity for the stability of PL suspension. Table 8.4 gives comparison of *in vitro* stability of PLs in the presence and absence of 10% sucrose.

The amount of tartaric acid present in PLs is ~50μg/mL and at this concentration we found no increase in impurity formation (7-epidocetaxel) during the 6 month of storage. The % EDTX content remained unchanged over a period of 6 months (0.462±0.112%) in the presence of tartaric acid.

Table 8.4. Comparison of *in vitro* stability of PLs in the presence and absence of 10% sucrose

Time (month)	% DTX retained	
	PLs without sucrose	PLs with 10% sucrose
Day -1	100	100
1	78.95±2.72	96.08±1.56
2	81.04±0.56	98.81±4.7
4	79.46±0.9	99.45±0.5
6	58.4±0.57	81.3±7.82

Values are Mean±SD, n=3. PLs: PEGylated liposomes. The PEGylated liposomes containing no sucrose showed significant decrease in DTX loading just after one month of storage at 2-8 ^{0}C ($p<0.0001$). Whereas, the PEGylated liposomes containing 10% sucrose showed significant decrease in DTX loading after 6 months of storage at 2-8 ^{0}C ($p<0.01$, $p=0.003$).

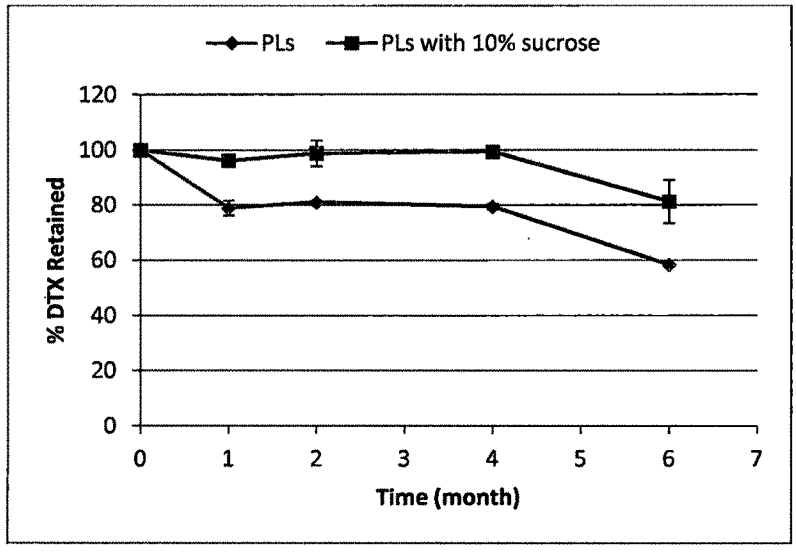

Figure 8.7. Comparison of *in vitro* stability of PLs in the presence and absence of 10% sucrose

8.12.6. *In vitro* cytotoxicity assay

We evaluated the cytotoxic effects of commercial formulation Taxotere and DTX loaded CLs, PLs, and PILs against human lung adenocarcinoma cell line (A549) and mouse melanoma cell line (B16F10). Cells were exposed to the drug formulations for 24hr, 48hr and 72hr and cell viability was determined. All formulations resulted in concentration dependent and time dependent inhibition of the proliferation of A549 (Figure 8.8) and B16F10 cells (Figure 8.9).

The lowest cell viability, i.e. the highest cell mortality, appeared at the highest concentration of the liposomal formulations after treatment for the longest time, which proves the controlled and sustained efficacy of the liposomal formulation. Furthermore, the liposomal formulations prevent the toxic effect of the drug applied at high concentration of drugs and thus can increase the maximum tolerance dose (MTD). Such a high concentration of drug instantly exposed in blood is presumed to be toxic not only for the cancer cells but also for the normal cells since it has exceeded the suggested maximum tolerable level of docetaxel (2700ng/ml) (Feng et al., 2009). It is clear from the results that the PLs and PILs demonstrated higher cytotoxicity than the Taxotere formulation at the same drug concentration and exposure time, which means that for the same therapeutic effect, the drug needed for the PLs and PILs formulation could be much less than that for the Taxotere formation. Therefore, the development of the PLs and PILs thus can enhance the therapeutic effect as well as increase the MTD of docetaxel.

A quantitative evaluation of the *in vitro* therapeutic effect of a dosage form is IC50, which is defined as the drug concentration needed to kill 50% of the incubated cells in a designated time period. The IC_{50} value after 24hr treatment of A549 cells is found high for Taxotere (25±4.082nM) than PLs (0.5±0.01nM) and PILs (3.52±0.521nM). Therefore PLs (50 times) and PILs (7.1 times) showed high therapeutic effectiveness as compared to Taxotere. After 48hr and 72hr of treatment the IC_{50} values decreased as compared to 24hr and remain almost same for Taxotere, PLs, and PILs (Table 8.5). This indicates Taxotere, PLs and PILs are almost equally effective after 48hr and 72hr treatment. The CLs showed higher IC_{50} values than Taxotere at all time points indicating less effective than Taxotere. This low cytotoxicity can be attributed to the low amount of DTX loaded in more amount of lipid leading to more time to diffuse and come in contact with the cells.

In case of B16F10 cells the IC_{50} values were shifted to higher values after 24hr of treatment as compared to A549 cells indicating B16F10 melanoma cells are less sensitive than A549 cells. After 48hr and 72hr of treatment the IC50 values PLs and PILs almost matches with the IC_{50} values against A549 cells. Both PLs and PILs showed lower IC_{50} values than Taxotere at all time points against B16F10 cells and this indicates PLs and PILs are remain more effective than marketed Taxotere. The CLs again showed higher IC_{50} values than Taxotere after 48hr and 72hr time points indicating less effective than Taxotere.

The PILs showed higher IC_{50} values (3.52±0.521) than PLs (0.5±0.01nM) after 24hr treatment against A549 cells. The PILs showed lower IC_{50} values after 24hr (1800±209nM) and 48hr (0.007±0.002nM) of treatment against B16F10 cells as compared to PLs (4000±807nM after 24hr treatment and 0.009±0.001nM after 48hr treatment). This indicates that the PILs are more effective against B16F10 than A549 cells. This might be due to difference in the expression of neuropilin-1 receptor between these two cells. From western blotting and FACS results of neuropilin-1 expression, it is very clear that the B16F10 showed more expression of neuropilin-1 than A549 with respect to total β tubulin content. Therefore, this might be the reason for more effectiveness of PILs against B16F10 (more uptake of PILs *via* receptor mediated endocytosis) than A549 cells (less expression might delay the uptake). Also, the presence of hydrophilic ligands (conjugated antibodies and cysteine molecules) at the distal end of the PEG chain may hinder the uptake more than PEG alone when neuropilin 1 receptors are available in very less number leads to less uptake *via* receptor mediated endocytosis and thereby less effectiveness of the PILs.

Against both the cell lines the PLs and PILs showed low IC_{50} values (more effective) than marketed Taxotere. These results are in accordance with previous studies that the cytotoxicity of drug loaded lipid based nanoparticles was higher than that of free drugs (Montero et al., 2005; Yanasarn et al., 2009). In many solid lipid nanoparticle (SLN) formulations less than half of the loaded drug is released during the cell cytotoxicity test, but these formulations are sometimes more cytotoxic to the cancer cells than the corresponding free drug. In other words, the cytotoxic compounds that remain unreleased and associated with the lipid based nanoparticles also appear effective (Wong et al., 2006; Serpe et al., 2004). Possible mechanism underlying the enhanced efficacy of DTX loaded nano structured lipid carriers (NLC) against cancer cells is that lipid nanoparticles may carry drug into the cancer cells by endocytosis and enhance intracellular drug accumulation by nanoparticle uptake (Wong et al., 2006a; Wong et al., 2006b). Therefore, the increased cytotoxicity of DTX loaded PLs and PILs compared to marketed Taxotere in our study can be better correlate to the reasons discussed above.

The cytotoxicity of blank PLs at different lipid concentrations was determined. The total lipid concentration used was similar to the CLs used to study the cytotoxicity of loaded DTX (1.5504μM, 155.04nM, 15.504nM, 1.5504nM, 0.15504nM, 0.015504nM, and 0.00155nM). We prepared the stock solution of blank PLs 1.2mg/mL (1.5504μM of total lipid) and further serial dilutions were made in culture medium and 100μL was added to each blank well.

The blank PLs had no effect on A549 and B16F10 cell growth at total lipid concentration of 15.504nM after all time points. Indeed, the differences in viability observed on cells that incubated with blank PLs and the non-treated cells were negligible. At higher concentrations of blank PLs (155.04nM and 1.5504μM) we observed both concentration and time dependent cytotoxicity against both the cell lines (Figures 8.8 and 8.9). Therefore, in our present study, the cytotoxicity of DTX loaded PLs (54nM of total lipid

at 10μM DTX solution) and PILs (59nM of total lipid at 10μM DTX solution) was carried out at the total lipid concentration which remains below toxic level (155.04nM) as compared to CLs. Therefore, the % viability of A549 and B16F10 observed at 1μM and 10μM of CLs loaded with DTX is because of both lipid and DTX, as lipids at this level also cause cytotoxicity.

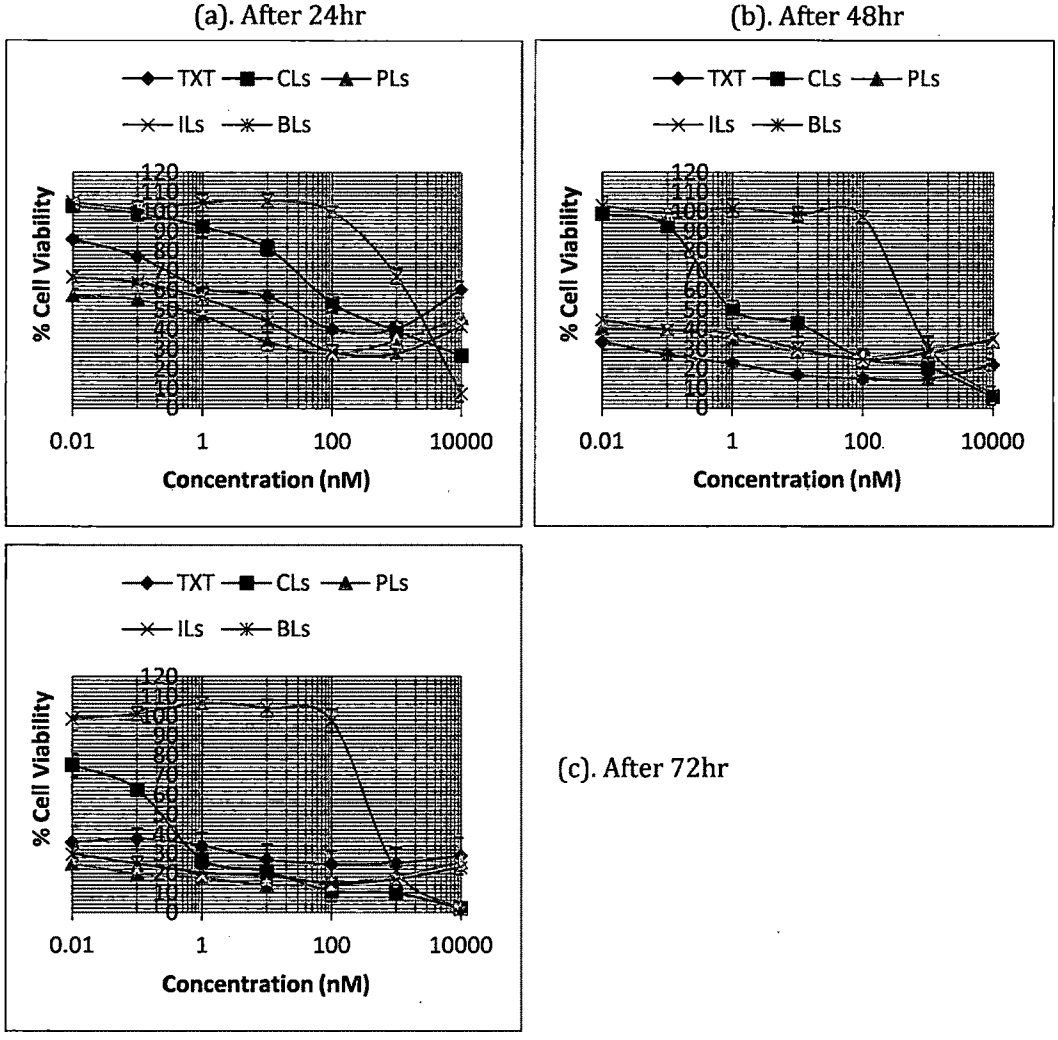

Figure 8.8. The % A549 cell viability after (a). 24hr, (b). 48hr and (c). 72hr of treatment with TXT, CLs, PLs, PILs, and BLs

(a). After 24hr

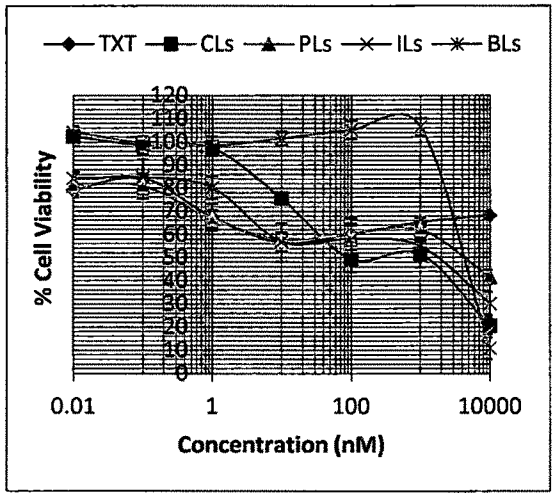

(b). After 48hr

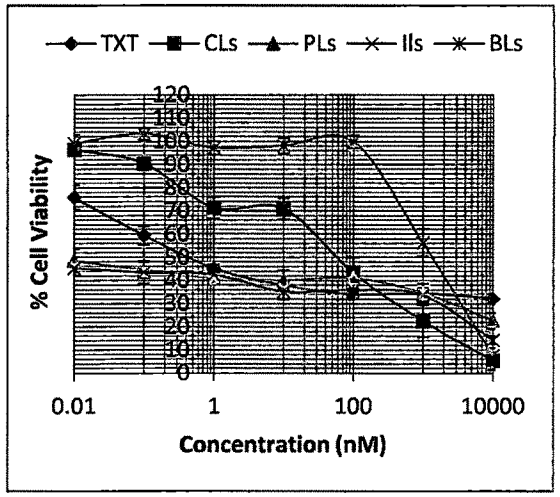

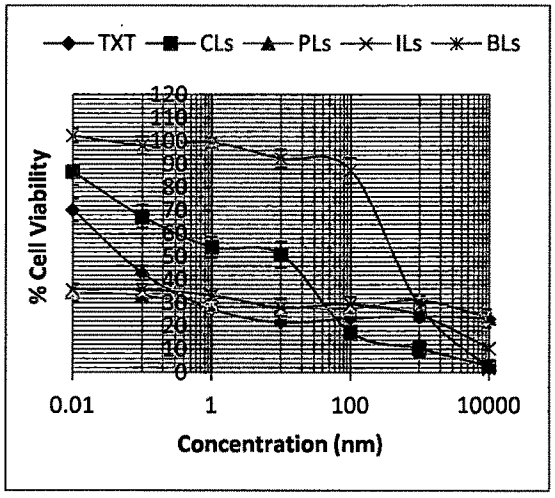

(c). After 72hr

Figure 8.9. The % B16F10 cell viability after (a). 24hr, (b). 48hr and (c). 72hr of treatment with TXT, CLs, PLs, PILs, and BLs

Table 8.5. The comparison of the IC_{50} values (nM) of TXT, CLs, PLs, and ILs against A549 and B16F10 cells at different time points

Drug	A549		
	24 hr	**48hr**	**72hr**
Taxotere	25±4.08	0.0051±0.0017	0.005±0.001
CLs	150±10	1.51±0.18	0.254±0.021
PLs	0.5±0.01	0.0064±0.001	0.004±0.0012
PILs	3.52±0.52	0.0071±0.002	0.0045±0.0015
Drug	**B16F10**		
Taxotere	not found	0.425±0.17	0.0512±0.013
CLs	90.67±11.67	60.73±5.76	10.63±2.48
PLs	4000±807	0.009±0.001	0.005±0.0012
PILs	1800±209	0.007±0.002	0.005±0.0015

Values are Mean±SD, n=3.

8.12.7. Cell uptake study

8.12.7.1. Using FACS

The quantitative uptake of 6-coumarin loaded liposomes was studied using FACS technique. The A549, B16F10 and K9 cell uptake of 6-coumarin loaded CLs, PLs, and ILs equivalent to 25μg and 50μg was shown in Figures 8.10, 8.11 and 8.12, respectively. The % relative mean fluorescence intensity (% RMFI) of these cell lines after uptake of CLs, PLs, and PILs was determined by considering the MFI of cells treated with CLs as 100% uptake and the calculated quantitative uptake values (% RMFI) are tabulated in Table 8.6 and Figure 8.13. The uptake of CLs (non-PEGylated) was found very rapid in all cell lines tested and also, it is very clear from the results obtained that the uptake of PLs and PILs was significantly decreased as compared to CLs in all cell lines tested. This result confirms the presence of hydrophilic PEG barrier on PLs and ILs preventing their rapid uptake by these cell lines.

The conjugation of Fab' fragment of anti-neuropilin 1 antibody over PLs can enhance the cell uptake *via* receptor mediated endocytosis. In case of A549 cell line we observed slightly increased uptake of PILs as compared to PLs. About 7-9% increase in RMFI was observed at lower concentration (25μg) for 30 and 60 minute incubation as compared to higher concentration of 50μg (about 4-5% increase in RMFI) (Table 8.6). In case of B16F10 cell line we observed increased uptake of PILs than PLs as compared to A549

cell line. This might be due to more expression of neuropilin-1 receptors on B16F10 as compared to A549 (from western blotting and FACS results of neuropilin 1 expression). About 16-20% increase in RMFI was observed for PILs at lower concentration of 25μg as compared to PLs. At higher concentration of 50μg, we observed about 8-13% increase in RMFI of B16F10 cells treated with PILs as compared to PLs. It is very clear from the results that at lower concentration we can clearly distinguish the uptake of PLs and PILs than at higher concentrations. Also, our results indicate the uptake of Fab' fragments conjugated PLs (PILs) by A549 and B16F10 cells *via* the receptor mediated endocytosis. The conventional liposomes are rapidly taken up by liver and spleen before reaching the target tissue. Hence, we tested the uptake of prepared CLs, PLs, and PILs using rat normal liver cell K9 and also from these *in vitro* results we can predict the *in vivo* status of prepared liposomes. The hydrophilic PEG barrier decreased the K9 cell uptake of PLs and PILs as compared to CLs in the similar passion to A549 and B16F10 cells (Figure 8.12 and Table 8.6). The uptake of PILs was found similar (at higher concentration of 50μg) to PLs or found decreased slightly (about 5%) at lower concentration of 25μg as compared to PLs. This decreased or similar uptake of PILs by K9 cells is might be due to the non-availability of neuropilin 1 receptors on K9 cells. Also, the presence of Fab' fragments and cysteine molecules (hydrophilic molecules) over the liposome surface might hinder the uptake by K9 cells as compared to PLs containing no surface attached molecules. The about 45% decrease in RMFI (45% decreased uptake by K9 cells) of K9 cells treated with PILs, as compared to CLs (100%) and PLs (40% decrease), indicates that the PILs would less uptake by liver and spleen *in vivo* leading to increased circulation half time and increased accumulation at tumor tissue. Also, from the *in vitro* results of PILs uptake by A549 and B16F10 cells, we can expect more uptake of PILs *via* receptor (neuropilin 1) mediated endocytosis at the tumor site as compared to PLs.

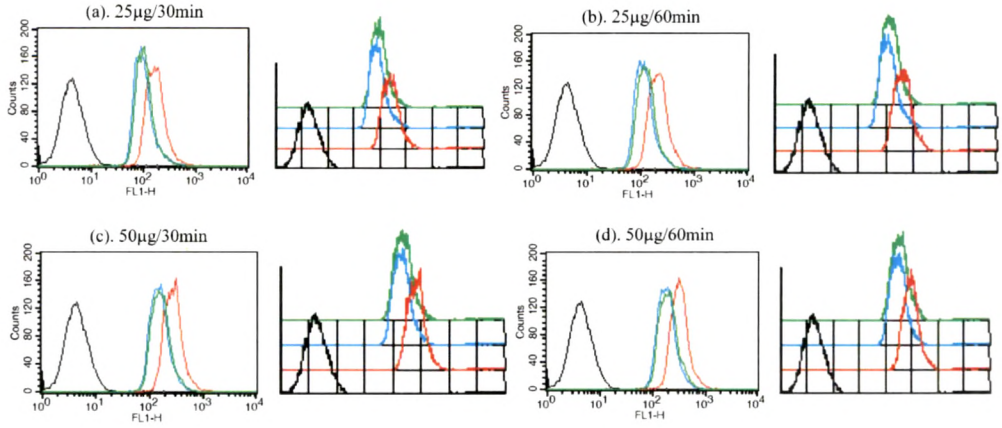

Figure 8.10. A549 cell uptake of 6-coumarin loaded CLs, PLs, and ILs

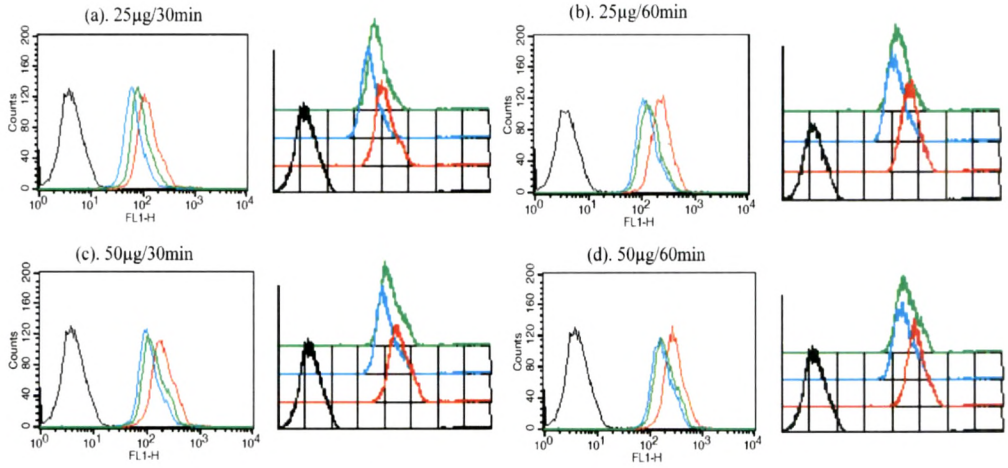

Figure 8.11. B16F10 cell uptake of 6-coumarin loaded CLs, PLs, and PILs

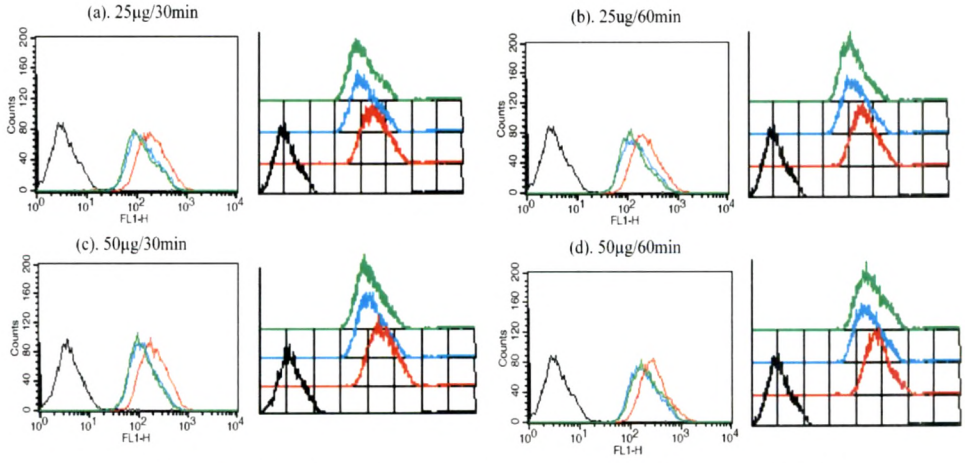

Figure 8.12. K9 cell uptake of 6-coumarin loaded CLs, PLs, and PILs

Table 8.6. The % relative mean fluorescence intensity (RMFI) of A549, B16F10 and K9 cells treated with different concentrations of 6-coumarin loaded CLs, PLs, and PILs for different time periods

	% RMFI of different cell lines			
A549	25μg/30min	25μg/60min	50μg/30min	50μg/60min
CLs	100	100	100	100
PLs	59.1±1.18	56.4±1.64	61.3±2.38	54.6±1.22
PILs	66.3±2.77	65.5±5.18	66.4±3.71	58.8±1.83
B16F10				
CLs	100	100	100	100
PLs	46.3±4.77	54.4±5.13	50.46±2.35	50.1±5.18
PILs	66.8±1.86	70.08±3.62	63.9±4.18	58.02±2.32
K9				
CLs	100	100	100	100
PLs	57.3±5.28	60.7±4.55	63.9±5.93	57.8±3.32
PILs	52.7±3.1	56.06±4.82	60.7±2.37	55.1±1.32

Values are Mean±SD, n=3. The A549, B16F10 and K9 cells showed significantly decreased uptake of PEGylated liposomes and immunoliposomes ($p<0.0001$) as compared to conventional liposomes at all concentrations and incubation time points tested. The immunoliposomes were significantly up taken by A549 cells ($p<0.05$: at 25μg/30mim, 25μg/60min and 50μg/60min) and B16F10 cells ($p<0.01$: at 25μg/30mim, 25μg/60min and 50μg/30min) as compared to PEGylated liposomes.

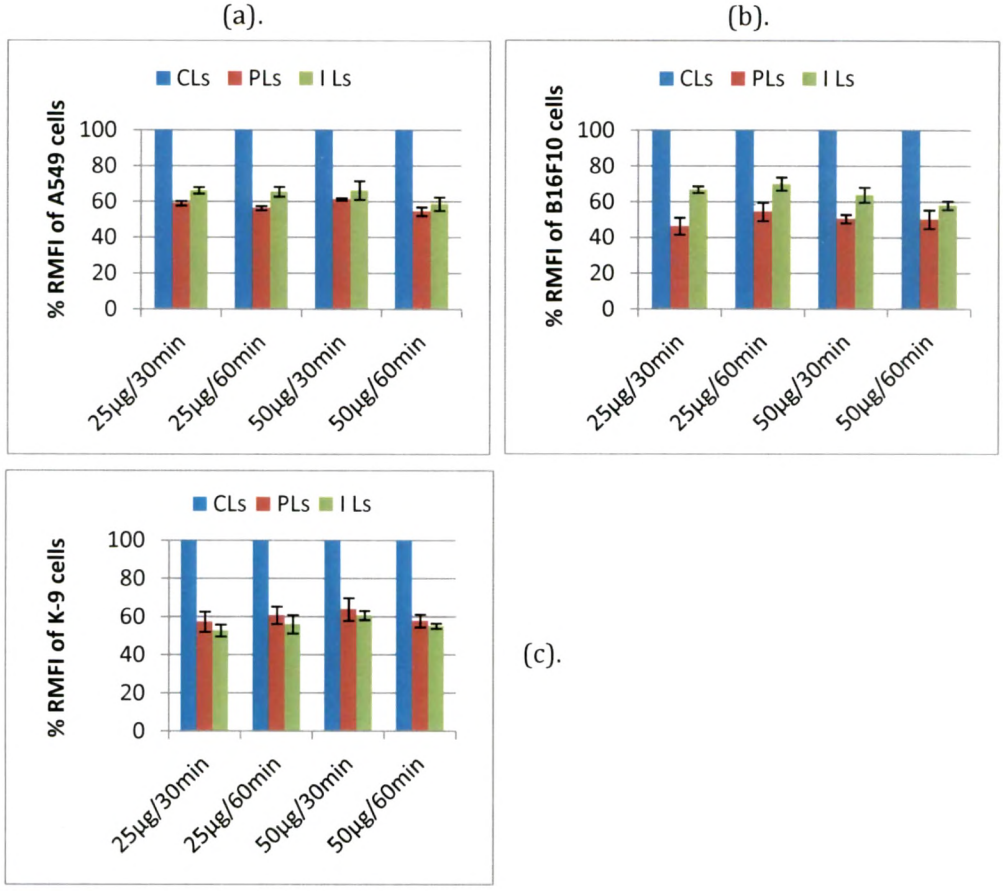

Figure 8.13. Comparison of % relative mean fluorescence intensity of (a). A549, (b). B16F10 and (c). K9 cells after incubation with 6-coumarin loaded CLs, PLs, and PILs equivalent to 25µg and 50µg of total phospholipid for a period of 30 and 60 minutes.

8.12.7.2. Using confocal microscopy

The qualitative uptake of CLs, PLs and PILs by A549, B16F10 and K9 cells was studied by confocal microscopic technique (Figures 8.14, 8.15 and 8.16). The confocal microscopic images reveal that the uptake is concentration and time dependent. We observed increased uptake with increase in concentration (from 25µg to 50µg) and incubation time (from 30 to 60 minutes). The confocal images depict increased uptake of CLs as compared to PLs and PILs. Also, we can observe the increased uptake of PILs in A549 and B16F10 cells as compared to PLs (Figure 8.14 and 8.15). Similarly, the less uptake and/or equal uptake of PILs by K9 cells as compared to PLs was observed (Figure 8.16).

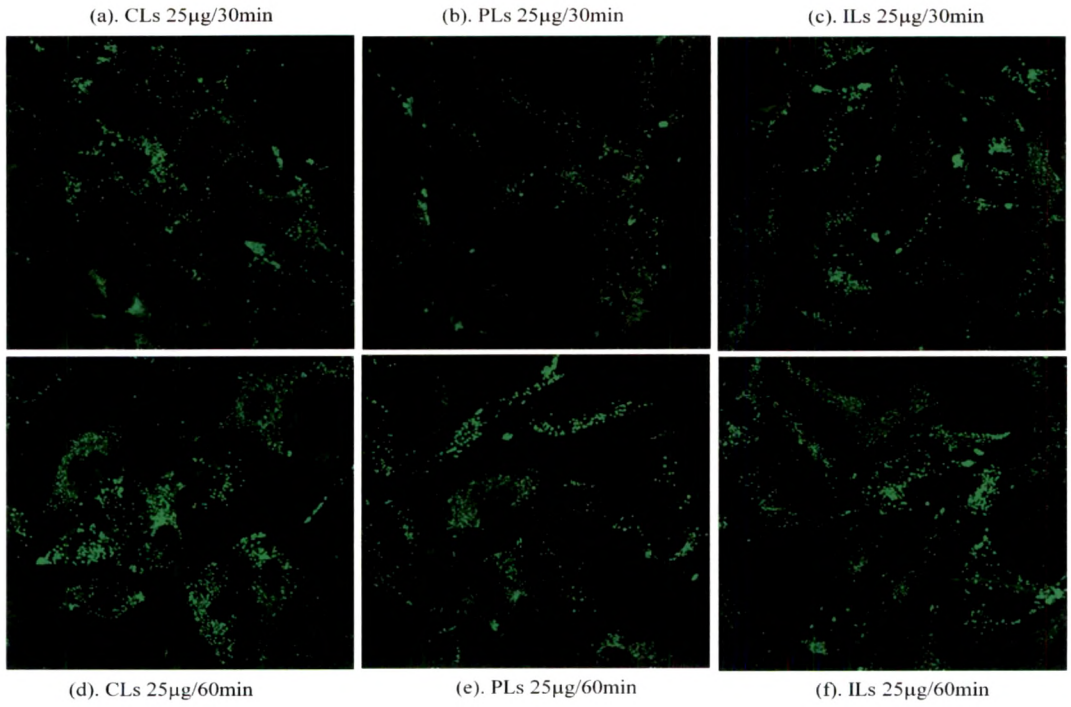

Figure 8.14. Confocal microscopic images of A549 cells after incubation with 6-coumarin loaded CLs, PLs, and PILs equivalent to 25µg of total lipid for a period of 30 and 60 minutes

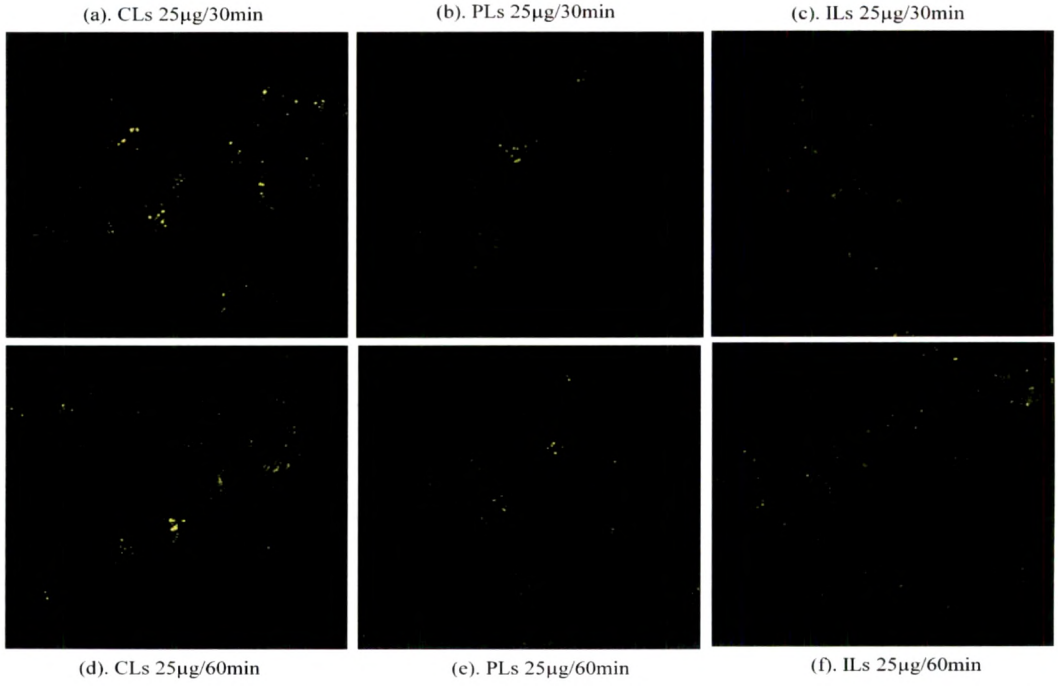

Figure 8.15. Confocal microscopic images of B16F10 cells (pseudo color given) after incubation with 6-coumarin loaded CLs, PLs, and PILs equivalent to 25µg of total lipid for a period of 30 and 60 minutes

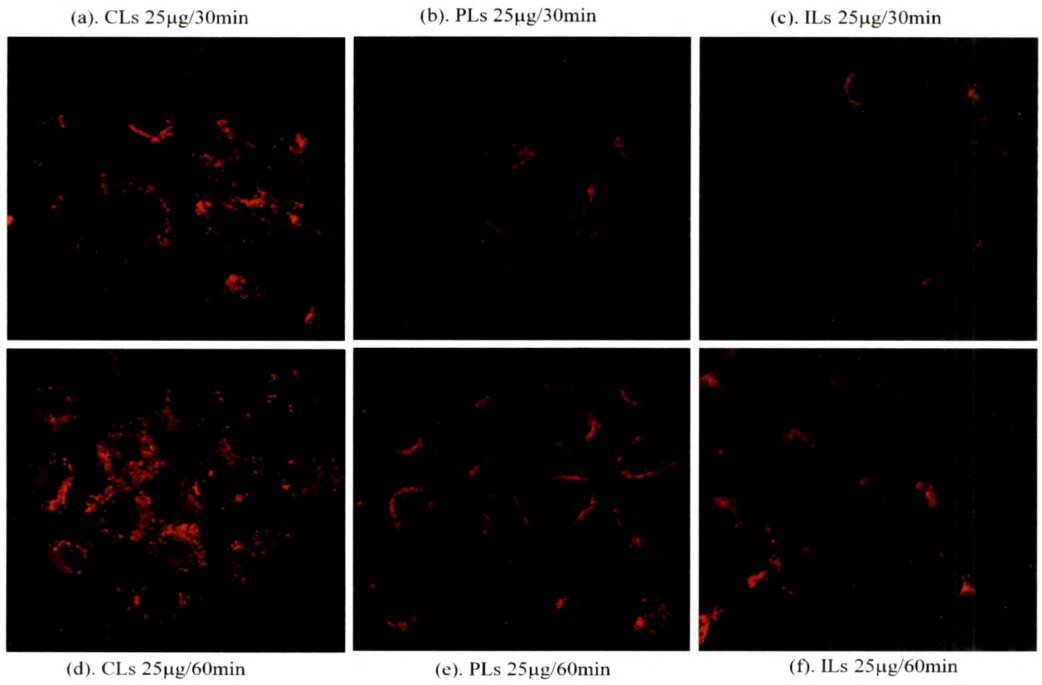

Figure 8.16. Confocal microscopic images of K9 cells (pseudo color given) after incubation with 6- coumarin loaded CLs, PLs, and PILs equivalent to 25µg of total lipid for a period of 30 and 60 minutes.

8.12.7.3. Live uptake imaging using confocal microscope

The conventional liposomal (CLs) uptake was represented in green color in the video. In the video it can be clearly seen that the A549 cells showed an immediate and rapid uptake of CLs equivalent to 25µg of total lipid (Video 1: see the CD attached with thesis). The liposomes are readily distributed throughout the cells and saturation occurs in a short time period. Thus, as the time increases (till 15 minutes) there is no much change in the fluorescence intensity was observed indicating early saturation of cells with CLs.

The PEGylated liposomal (PLs) uptake was represented in yellow color (given pseudo color) in the video (Video 2). In contrast, the A549 cells showed slow uptake of PLs equivalent to 25µg of total lipid. We observed no immediate saturation as observed with CLs and the fluorescence (PLs uptake) increases with increase in time. However, no increase in the fluorescence intensity was observed at the end of 15 minutes. This observation confirms the fact that the PEGylation alters the binding affinity to the cellular surface and thus liposomal uptake.

In case of anti-neuropilin-1 immunoliposomes (PILs), video showed (pseudo color red given) a very precise uptake. Upon addition of PILs the liposomes gets clustered around the A549 cells surface slowly with respect to time. The fluorescence intensity increases as the number of liposomes at cell surface increase with time. At the end of 15 minutes,

we observed more number of liposomes attaché at the cell surface but not internalised by the cells (Video part 1). However, with increasing time (after 15 minutes) we observed internalisation of surface attached immunoliposomes (Video Part 2, till 25 minutes).

Initially, the PILs took time to find and bind their receptors on the surface of A549 cells. After binding to their receptors, during the second half, PILs are completely internalised and gets distributed into the cells. As a result the nucleus of cells becomes more distinct since PILs get clustered around the nuclear membrane. The *in vitro* live imaging revealed the very clear specificity of the PILs to their target. Hence, it clearly indicates their potential applications in the field of translational therapeutics making the dream of a pharmacologist "From bench to bedside" realistic and possible.

8.12.8. Anti-metastatic activity by wound scratch assay

Migration is one of the key features in cancer progression involved in dissemination of tumor cells from its origin to a distant site (Friedl and Wolf, 2003). Rho GTPases are one of the key determinants involved in regulating migration by affecting actin cytoskeleton as well as influencing microtubular network (Etienne-Manneville and Hall, 2002). Microtubules consequently tone the activities of these Rho GTPases as well (Watanabe et al., 2005). Docetaxel has been shown to inhibit Cdc-42, one of the key members of Rho GTPase family in head and neck cancers (Kogashiwa et al., 2010). Further, docetaxel also inhibits endothelial cell migration (Murtagh et al., 2006; Grant et al., 2003). Based on these reports we have tested the *in vitro* anti-migratory effect of Taxotere and DTX loaded PLs and PILs, by wound scratch assay, against human lung adenocarcinoma cell line A549 (Figure 8.17) and mouse melanoma cell line B16F10 (Figure 8.18). According to this assay the anti-migratory effect of a drug is indirectly proportional to % wound covered as compared to untreated cells. The lesser the wound covered in treated cells as compared to untreated cells indicates that the drug has a good anti-migratory effect against the tested cell lines.

The wound width was measured using the Carl Zeiss Axiovision Rel 4.8.2 imaging software and the results were presented as percent wound covered by considering the control group width as 100% wound covered (Figure 8.19). In A549 cells we observed 81.76±8.16% and 60.51±3.01% of covered wounds at sub-toxic dose of 1nM and 2nM of Taxotere, respectively. The PLs showed more covered wounds, less antimigratory effect, than marketed Taxotere at the similar doses of 1nM (90.84±6.61%) and 2nM (70.64±6.77%). However, with PILs observed very less covered wounds, more anti-migration effect, than Taxotere and PLs at the similar doses of 1nM (77.78±8.57%) and 2nM (44.66±6.6%). Similarly, against B16F10 cells we observed 80.72±3.08% and 64.24±8.46% of covered wounds at sub-toxic dose of 1nM and 2nM of Taxotere, respectively. The PLs showed almost same % of wound covered at the similar doses of 1nM (82.32±5.63%) and 2nM (59.49±9.76%). However, with PILs, we observed very less covered wounds, more antimigratory effect, than Taxotere and PLs at the similar doses of 1nM (73.04±12.94%) and 2nM (53.77±2.08%). We observed no significant

difference in antimigratory effect of Taxotere and PILs against A549 and B16F10 at the tested dose of 1nM and 2nM. However, the about 10% increased anti-migratory effect of PLs was observed against B16F10 as compared to A549 cells.

As per the Ochiumi et al. report, it is clear that the neuropilin-1 receptors are involved in the regulation of migration of colon cancer cells (Ochiumi et al., 2006). Therefore, the significant anti-migratory effect against both the cell lines tested was observed in our study with anti-neuropilin-1 conjugated immunoliposomes is might be due to rapid uptake of PILs *via* neuropilin-1 receptors, expressed on A549 and B16F10 cells, and release of loaded DTX in the cells cytosol. The released docetaxel will affect the microtubules network (Kogashiwa et al., 2010; Etienne-Manneville and Hall, 2002) and thus might affect cell migration. There is no significant difference in % wound covered was observed between untreated cells (A549 and B16F10) and cells (A549 and B16F10) treated with 2mL of 1μg/mL neuropilin-1 antibody solution (95.21±3.91%). This indicates the antibodies have no anti-migratory effect against tested neuropilin-1 expressing A549 and B16F10 cells. This also confirms the significant anti-migratory effect observed with PILs is because of rapid uptake of PILs *via* neuropilin 1 receptors and not because of conjugated neuropilin-1 antibody itself.

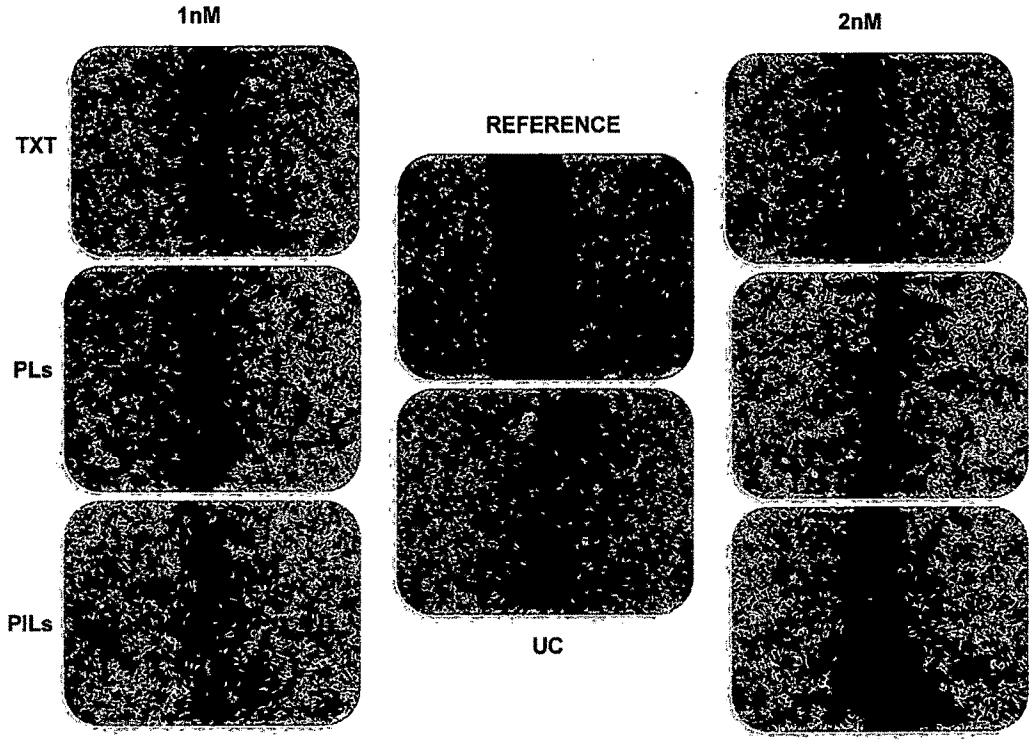

Figure 8.17. Zeiss Axio Inverted Microscopic images showing migration of A549 cells in the presence of different concentrations of Taxotere, DTX loaded PLs and PILs.

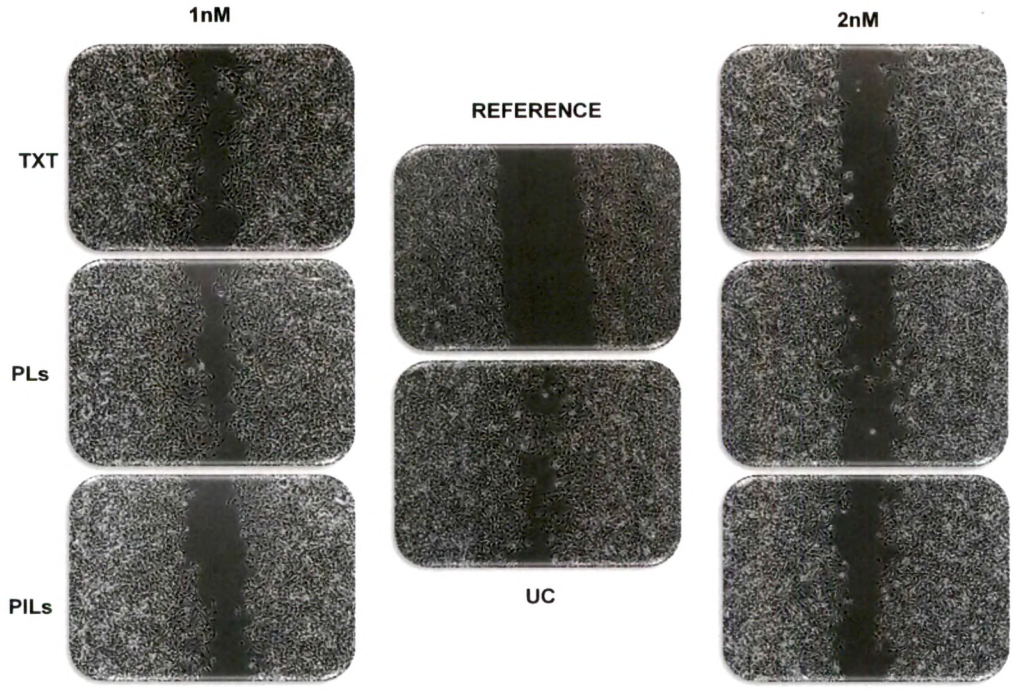

Figure 8.18. Zeiss Axio Inverted Microscopic images showing migration of B16F10 cells in the presence of different concentrations of Taxotere, DTX loaded PLs and PILs.

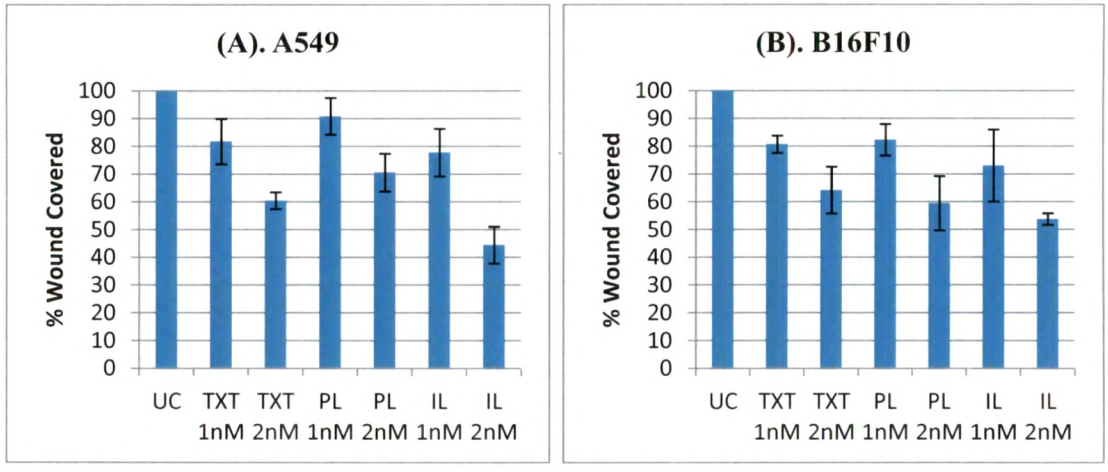

Figure 8.19. The % wound covered in the presence of different concentrations of Taxotere and DTX loaded PLs and PILs. Values represented are Mean±SD, n=3.
The Taxotere ($p<0.0001$), PLs ($p<0.001$) and PILs ($p<0.0001$) showed significant anti-metastatic activity, against A549 cells, at 2nM concentration as compared to untreated cells. The PILs showed significant anti-metastatic activity against A549 cells ($p<0.01$, $p=0.004$) as compared to PEGylated liposomes. Similarly, the Taxotere ($p<0.001$), PLs ($p<0.0001$) and PILs ($p<0.0001$) showed significant anti-metastatic activity against B16F10 cells at 2nM concentration as compared to untreated cells.

8.12.9. Gelatin zymography

Hong et al. [Hong et al., 2007] showed that Nrp1 knockdown in lung cancer cell lines reduced their ability to migrate, invade and form filipodia, and it also inhibited metastasis. Furthermore, NRP1 plays a role in potentiating the effect of HGF (hepatocyte growth factor)/Scatter factor signalling through the c-Met receptor in both glioma and pancreatic cancer cell lines, regulating tumour progression and invasion (Hu et al., 2007; Matsushita et al., 2007). These findings taken together with the expression of NRPs in diverse neoplasms, suggests a possible role for this molecule in tumour invasion and metastasis in addition to its involvement in tumour vascularisation. The precise mechanisms of action of NRPs in cancer are difficult to pinpoint, because they interact with so many cancer-associated molecules (Prud'homme and Glinka, 2012; Ellis, 2006). Thus, they could be contributing to cancer cell proliferation, migration, invasion, adhesiveness and metastasis.

Matrix metalloproteinases (MMPs) are one of the major key players in the process of tumor development (Polette et al., 2004; Kessenbrock et al., 2010). Among the major families of MMPs, MMP-2 and MMP-9 are the major gelatinases (Egeblad and Werb, 2002). Gelatin is a by product of collagen which is one of the major constituents of basement membrane (Pöschl et al., 2004). Thus, for tumor cells to escape into the bloodstream they need to degrade this barrier of basement membrane.

Therefore, in the present study, we have tested the interaction of docetaxel, docetaxel loaded PEGylated liposomes, and anti-neuropilin-1antibody (Fab' fragment) conjugated PEGylated liposomes (Anti-neuropilin-1 immunoliposomes) with MMPs of human adenocarcinoma cell line (A549) and mouse melanoma cell line (B16F10) to determine their role in tumor invasion and metastasis.

The human A549 cells showed higher activity of MMP-2 than MMP-9 (Figure 8.20A). This result was in accordance with previous findings which clearly revealed that the MMP-2 is a more predictable marker of lung cancer confirmed by immunostaining and elevated serum levels (Guo et al., 2007). The mouse B16F10 melanoma cells showed higher levels of MMP-9 and very weak bands were observed for MMP-2 (Figure 8.20B). It has been reported that the higher serum levels of MMP-9 in melanoma is inversely proportional to patients survival rate (Nikkola et al., 2005).

The zymograms of A549 and B16F10 cells treated with docetaxel, and docetaxel loaded PEGylated liposomes and anti-neuropilin-1 immunoliposomes showed no changes in the activity of both endopeptidases (Figure 8.20A and 8.20B). The densitometry analysis of bands also showed minimal changes in band intensities of docetaxel and docetaxel loaded liposomes treated cells as compared to untreated sample. These results clearly suggest that docetaxel and docetaxel loaded liposomal formulations does not affect the activities of MMP-2 and MMP-9. However, it is quite possible that they might affect other molecules in the invasion process.

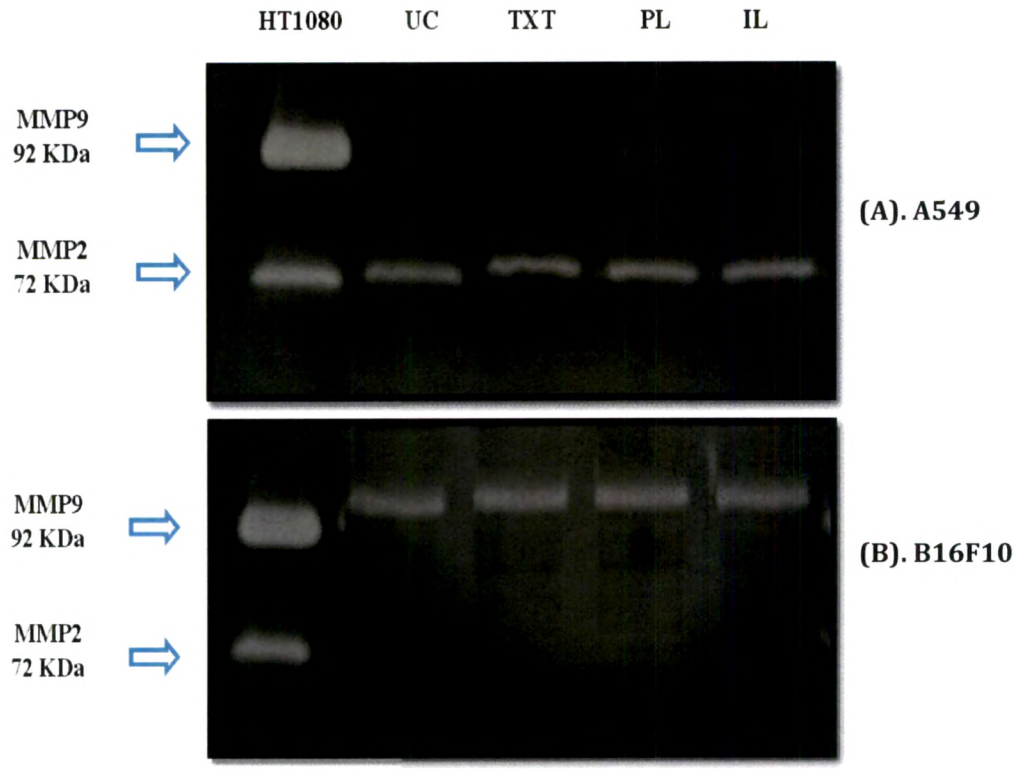

Figure 8.20. The comparison of interaction of docetaxel and docetaxel loaded PEGylated liposomes and immunoliposomes with MMP-9 and MMP-2 of (A). A549 cells and (B) B16F10 cells to determine their role in tumor invasion and metastasis

8.12.10. Apoptosis assay

8.12.10.1. Using FACS

The cells were stained with propidium iodide (PI) and flow cytometry was used to distinguish and quantitatively determine the percentage apoptotic cells. The 10000 events were collected and analysed using CellQuest software. The % A549 and B16F10 apoptotic cells gated (M_1), after treatment with 2nM of Taxotere, DTX loaded PEGylated liposomes and PEGylated immunoliposomes for a period of 24hr and 48hr was shown in Figure 8.21 and Figure 8.22, respectively.

We observed about 18.55±0.5%, 18.81±0.76%, and 19.23±2.4% of apoptotic A549 cells after 24hr treatment with 1mL of Taxotere, PLs, and PILs, respectively as compared to untreated cells (0.485±0.12%). About 16.7±4.65%, 25.42±4.44%, and 21.36% of apoptotic A549 cells were observed after 48hr treatment with 1mL of Taxotere, PLs, and PILs, respectively as compared to untreated cells (0.43±0.16%). No significant difference in % apoptosis was observed between Taxotere, PLs and PILs after 24hr treatment (Figure 8.23A). However, about 8.72% and 4.66% increased apoptosis was observed with PLs and PILs, respectively after 48hr treatment as compared to Taxotere. We observed no significant difference in A549 cell apoptosis caused by PLs and PILs.

Similarly, we observed about 3.66±0.43%, 3.87±0.71%, and 3.84±0.45% of apoptic B16F10 cells after 24hr treatment with 1mL of Taxotere, PLs, and PILs, respectively as compared to untreated cells (0.385±0.01%). About 6.33±0.9%, 7.02±0.77%, and 9.71±0.58% of apoptotic B1F10 cells were observed after 48hr treatment with 1mL of Taxotere, PLs, and PILs, respectively as compared to untreated cells (1.01±0.56%). No significant difference in % apoptosis was observed between Taxotere, PLs and PILs after 24hr treatment (Figure 8.23B). However, about 0.69% and 3.38% increased apoptosis was observed with PLs and PILs, respectively after 48hr treatment as compared to Taxotere. We observed about 2.69% increased apoptosis with PILs as compared to PLs after 48hr treatment. This increased apoptosis of B16F10 cells with PILs as compared to A549 cells is could be due to more expression of neuropilin-1 receptors with B16F10 cells as compared to A549 cells (as per our western blotting and FACS results of neuropilin-1 expression).

About 5.06, 4.86, and 5 fold increased apoptosis was observed with A549 cells as compared to B16F10 cells after 24hr treatment with Taxotere, PLs, and PILs, respectively. Similarly, about 2.63, 3.62, and 2.19 fold increased apoptosis was observed with A549 cells as compared to B16F10 cells after 48hr of treatment with Taxotere, PLs, and PILs. This increased apoptosis of A549 cells as compared to B16F10 cells indicates that the B16F10 cells are less sensitive than A549 cells.

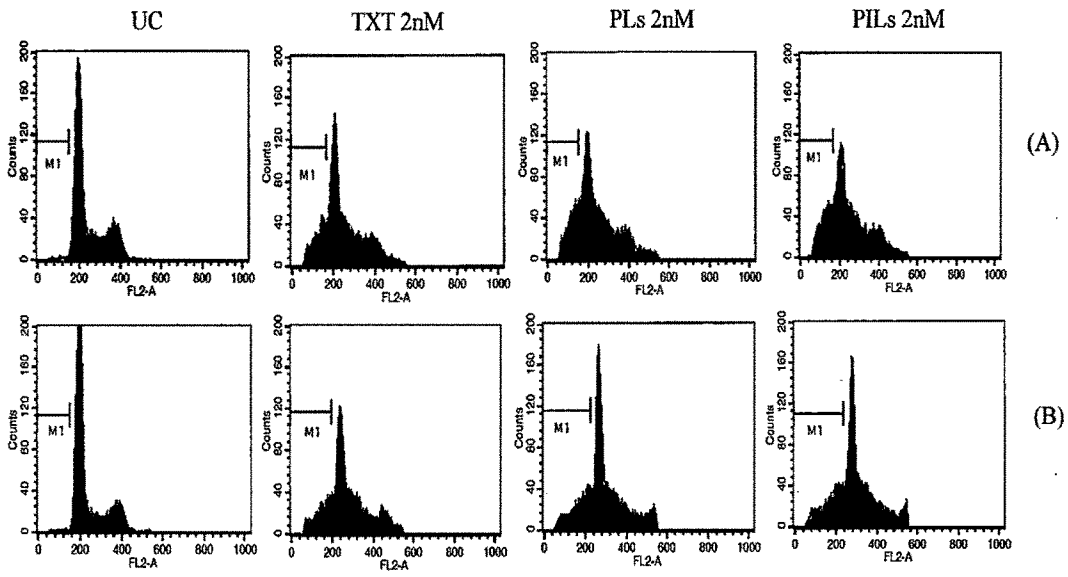

Figure 8.21. A549 cell apoptosis after treatment with TXT, PLs, and PILs of 2nM for 24hr (A) and 42hr (B).

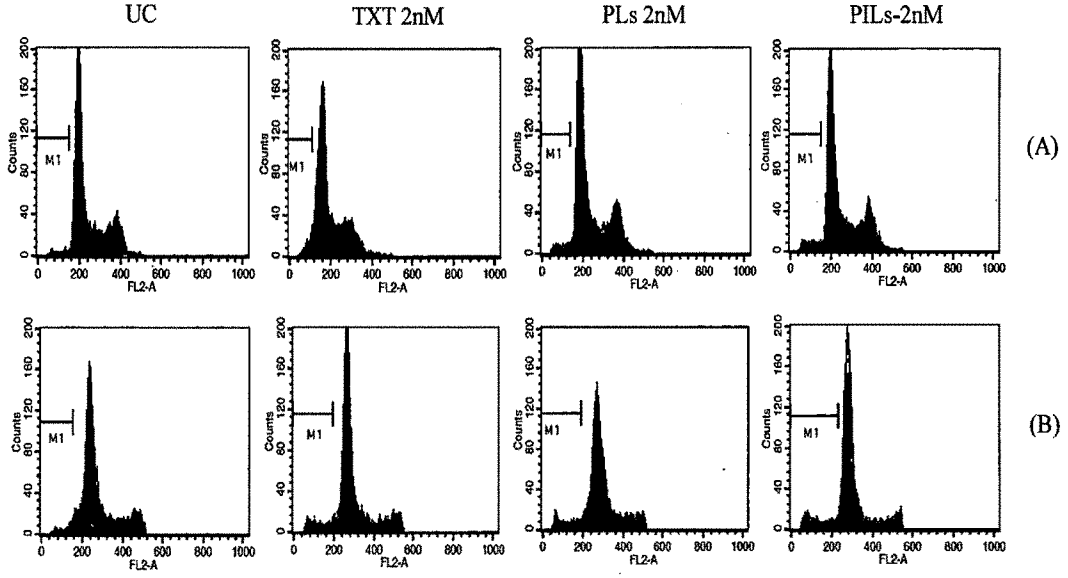

Figure 8.22. B16F10 cell apoptosis after treatment with TXT, PLs, and PILs of 2nM for 24hr (A) and 42hr (B).

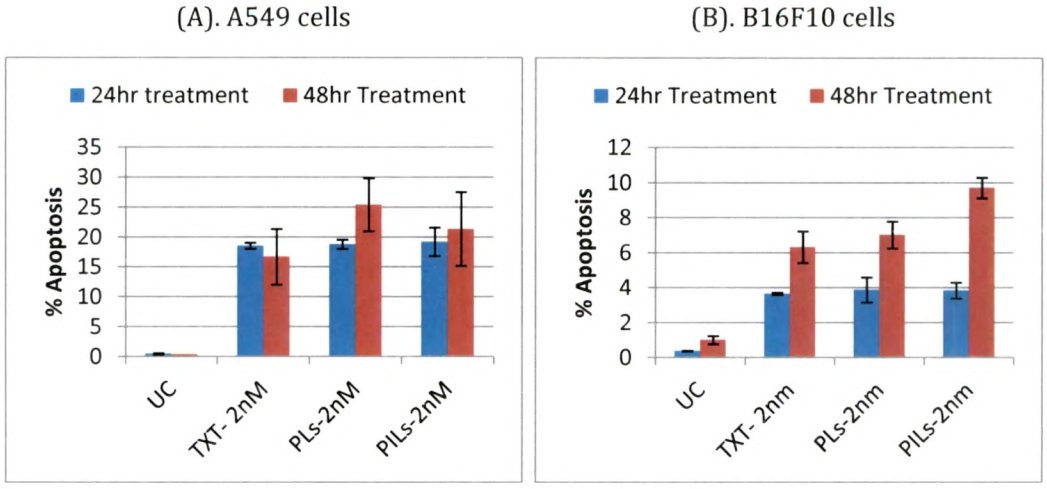

Figure 8.23. The % A549 (A) and B16F10 (B) cell apoptosis after treatment with 1mL of 2nM Taxotere, DTX loaded PEGylated liposomes (PLs) and PEGylated immunoliposomes (PILs) for a period of 24hr and 48hr.

The Taxotere, PLs and PILs caused significant apoptosis of A549 cells at 2nM concentration and after 24hr treatment as compared to untreated cells ($p<0.0001$). Similarly the 48hr treatment with 2nM concentration of Taxotere ($p<0.05$, 0.012), PLs ($p<0.01$, 0.001) and PILs ($p<0.01$, 0.001) also caused significant A549 cell apoptosis as compared to untreated cells.

The Taxotere, PLs and PILs caused significant apoptosis of B16F10 cells at 2nM concentration and after 24hr treatment and 48hr treatment as compared to untreated cells ($p<0.0001$). The immunoliposomes showed significantly increased B16F10 apoptosis as compared to Taxotere ($p<0.01$, $p=0.002$) and PLs ($p<0.01$, $p=0.007$) after 48hr of treatment.

8.12.10.2. Using EB/AO staining

Ethidium bromide/Acridine orange (EB/AO) staining is a very reliable method that can discriminate between live and dead cells (Ribble et al., 2005). The basic principle behind the assay is the differential staining properties of both dyes based on membrane integrity. The inclusion dye, Acridine Orange, penetrates the membrane of both live as well as dead cells while the latter Ethidium Bromide penetrates only the dead cells, intercalating into the DNA (Renvoize et al., 1998). The acridine fluoresces green in viable cells while ethidium bromide appears orangish red when intercalated into DNA. The EB/AO staining using microscopy is one of the best methods to distinguish *via*ble and non-viable cells compared to other conventional methods such as DNA fragmentation, Annexin-V, Tunel assay, Caspase assays and others (Ribble et al., 2005; Baskic et al., 2006). There are several reports that indicate the potential of the following method to determine the effect of anti-metastatic agents on several cancerous cells (Baskic et al., 2006; Goel and Gude, 2011; Polo et al., 2010).

The study addresses the apoptotic effect of docetaxel, and docetaxel loaded PLs and PILs on both human adenocarcinoma cell line A549 (Figure 8.24) and mouse melanoma B16F10 cells (Figure 8.25). This study provides an add-on validation of the results obtained using propidium iodide staining method using flow cytometry. From the figures it can be clearly seen that there is an increased apoptotic cells (appearing orange-reddish) with increase in time from 24hr to 48hr hours against both the cell lines (Figure 8.24 and 8.25). However, the effect is much more pronounced in case of human A549 cells as compared to B16F10 cells indicating A549 cells are more sensitive to treatment. Further, it can be seen that the docetaxel (Taxotere) is exhibiting lesser toxicity as compared to its liposomal counterparts which further corroborate the potential of controlled release delivery vehicles such as PLs and PILs. The PILs, as compared to PLs, showed slightly increased apoptosis against B16F10 cell lines as compared to A549 cells. This might be due to more and uniform expression of neuropilin-1 receptors over B16F10 cells as compared to A549 cells (from our western blotting and FACS results of neuropilin-1 expression).

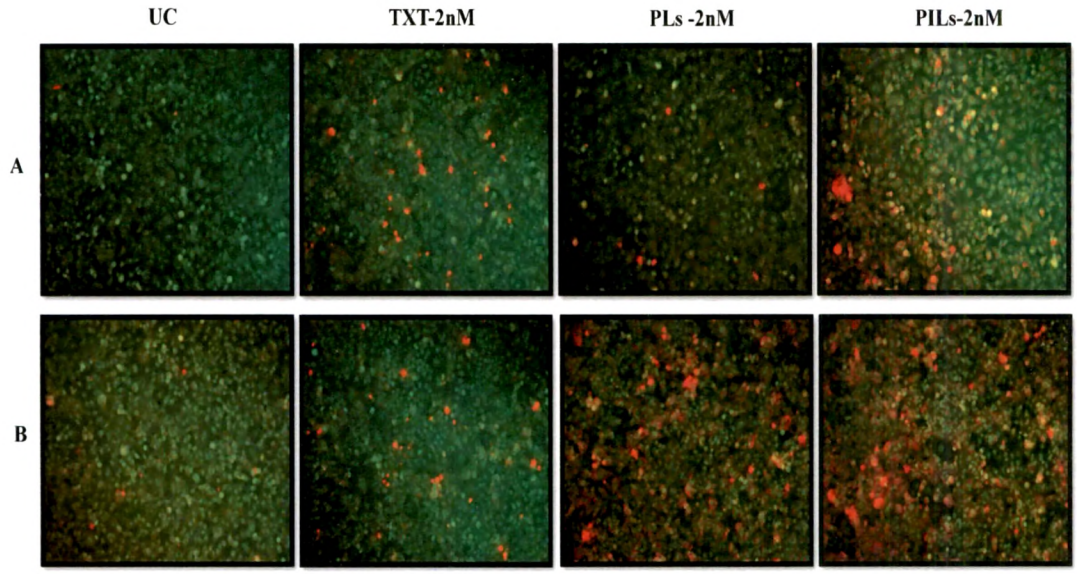

Figure 8.24. EB/AO staining of A549 cells after (A) 24hr and (B) 48hr treatment

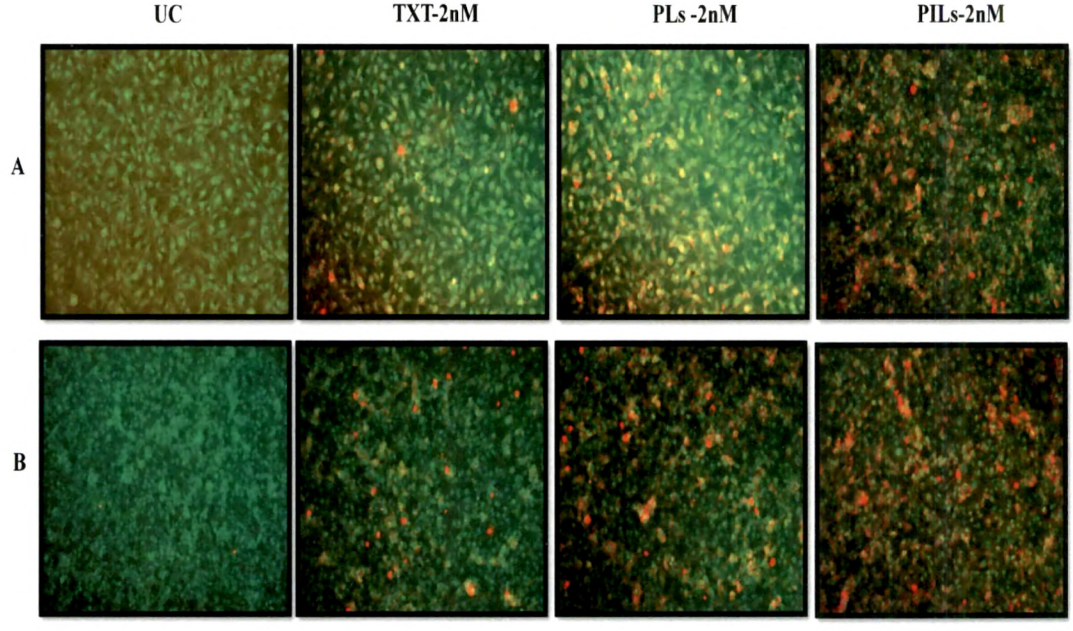

Figure 8.25. EB/AO staining of B16F10 cells after (A) 24hr and (B) 48hr treatment

8.12.11. Cell cycle analysis

To determine the effect of Taxotere and docetaxel loaded PLs and PILs on cell cycle, the A549 and B16F10 cells were treated with 2mL of 2nM solution of Taxotere and docetaxel loaded PLs and PILs for a period of 24hr and 48hr. The drug treated cells were then acquired on FACS Calibur and analysed using ModFit software to determine the percentage of A549 (Figure 8.26) and B16F10 (Figure 8.27) cells present in G0-G1, S and G2-M phase of cell cycle.

We observed about 60.14±1.13%, 29.34±0.62% and 10.52±0.71% of untreated A549 cells in G0-G1, S and G2-M phase, respectively after 24hr. Similarly, 76.17±6.92%, 16.71±5.44% and 7.09±1.53% of untreated A549 cells were observed in G0-G1, S and G2-M phase, respectively after 48hr (Table 8.7).

About 8.4% increased A549 cells at S phase were observed with PLs and PILs after 24hr treatment (Figure 8.28A). No changes were observed with Taxotere treated cells. Similarly, the about 10.37%, 19.37% and 26% increased A549 cells in S phase were observed after 48hr treatment with Taxotere, PLs and PILs, respectively (Figure 8.28B). Thus, the 9% and 15.63% increased accumulation of cells at S phase was observed with PLs and PILs, respectively as compared to Taxotere after 48 hr treatment. The PILs showed about 6.6% increased accumulation of cells at S phase as compared to PLs and this indicates the superiority of PILs over PLs.

The about 5.1% and 5.2% increase in A549 cells at G2-M phase was observed after 24hr treatment with Taxotere and PILs, respectively, whereas no change was observed with PLs. After 48hr treatment we observed about 4.7%, 1% and 5.4% decrease in G2-M phase with Taxotere, PLs and PILs, respectively.

In case of B16F10 cells, we observed about 63.54±12.7%, 24.46±15.5% and 11.99±2.9% of untreated cells at G0-G1, S and G2-M phase, respectively after 24hr. Similarly, the 76.26±10.95%, 17.04±9.3% and 6.69±1.5% of untreated B16F10 cells were observed in G0-G1, S and G2-M phase, respectively after 48hr (Table 8.8).

About 4.3% and 3.9% increased B16F10 cells at S phase was observed with PLs and PILs, respectively after 24hr treatment. Taxotere treatment caused about 4.7% decrease in S phase after 24hr and about 3.6% increase in S phase after 48hr. However, no changes in S phase were observed with PLs and PILs after 48hr treatment (Figure 8.29A and 8.29B).

About 4.5% increase in B16F10 cells in G2-M phase was observed after 24hr treatment with Taxotere, whereas PLs and PILs treatment caused about 1.5% and 1.3% decrease in G2-M phase, respectively. After 48hr treatment no change in G2-M phase was observed with Taxotere, whereas the PLs and PILs caused about 1.4% and 1.2% increase in G2-M phase, respectively. Our results clearly indicate that the mouse melanoma cell line (B16F10) is less sensitive at tested dose than human adenocarcinoma cell line (A549).

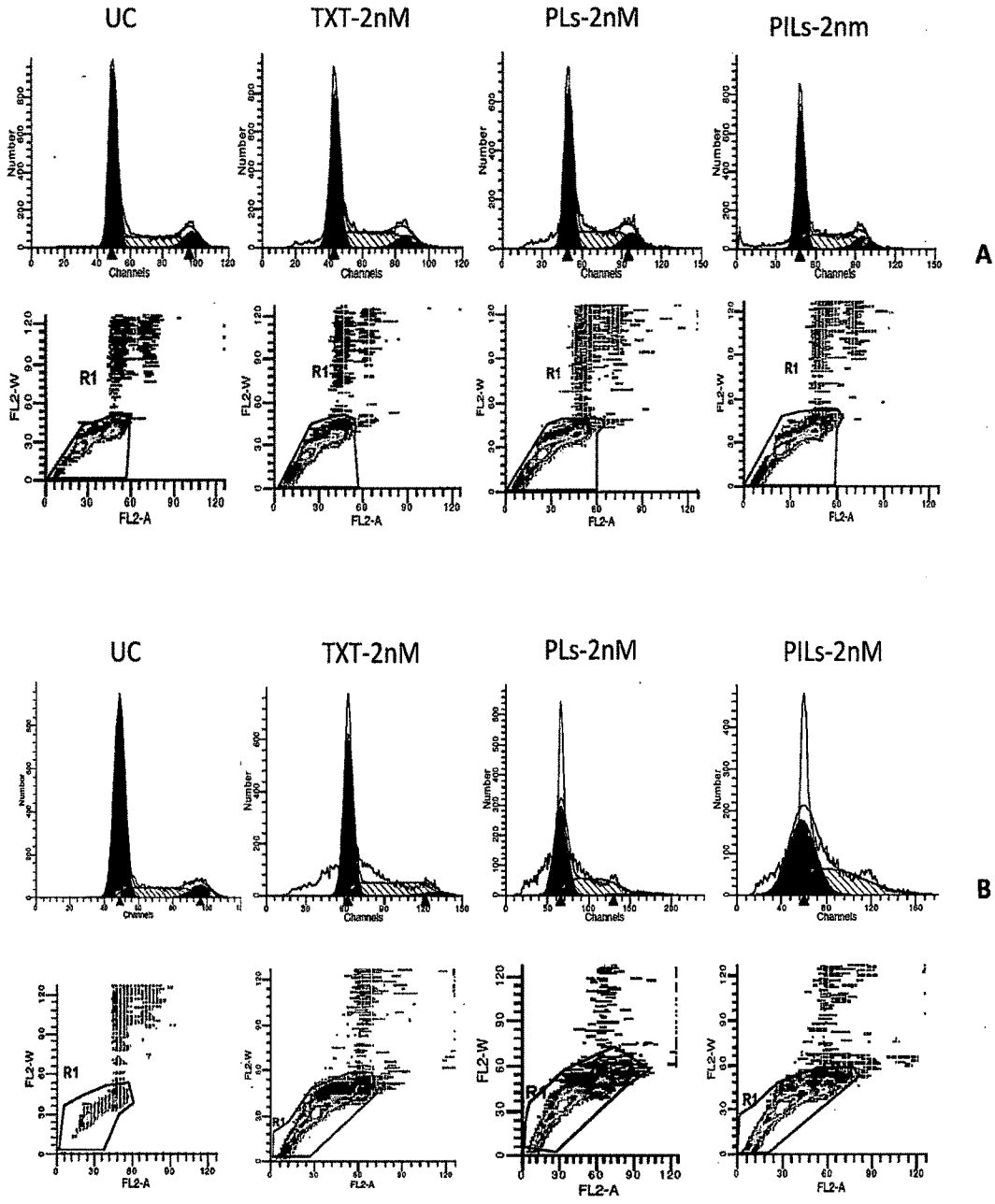

Figure 8.26. The FACS analysis of % A549 cells at G0-G1, S and G2-M phase after treatment with 2nM solution of Taxotere, PLs and PILs for a period of (A): 24hr and (B): 48hr.

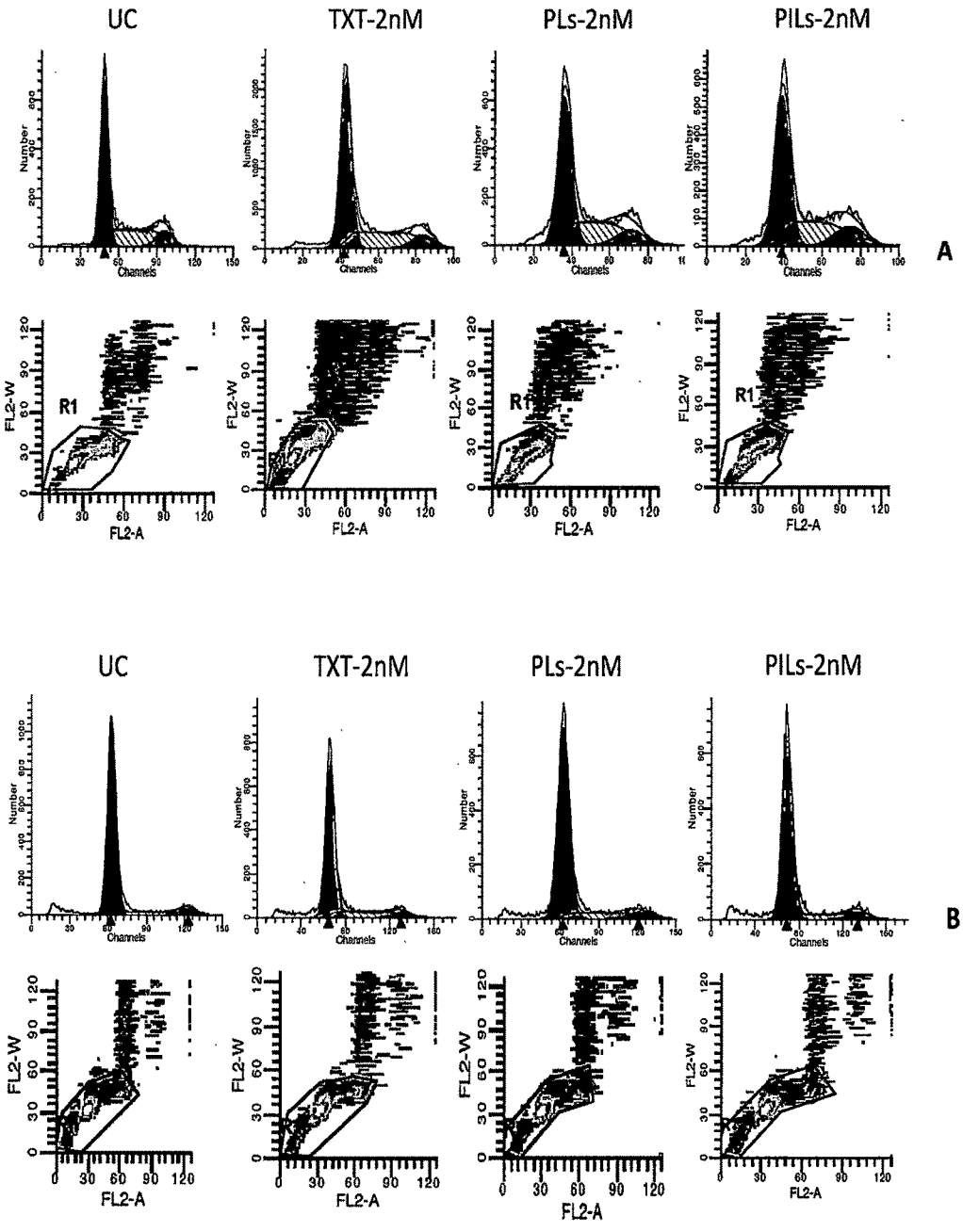

Figure 8.27. The FACS analysis of % B16F10 cells at G0-G1, S and G2-M phase after treatment with 2nM solution of Taxotere, PLs and PILs for a period of (A): 24hr and (B): 48hr.

Table 8.7. The % of A549 cells in G0-G1, S and G2-M phase after treatment with 2nM solution of Taxotere, PLs and PILs for a period of 24hr and 48hr.

Drug	After 24hr treatment			After 48hr treatment		
	G0-G1	S	G2-M	G0-G1	S	G2-M
UC	60.14±1.13	29.34±0.62	10.52±0.71	76.17±6.92	16.71±5.44	7.09±1.53
TXT 2nM	54.57±2.35	29.78±6.56	15.64±8.91	70.53±13.86	27.08±14.11	2.38±0.247
PLs 2nM	50.69±3.23	37.8±3.66	11.25±4.21	57.73±0.24	36.08±8.42	6.19±3.13
PILs 2nM	53.58±4.37	37.79±5.11	15.74±10.25	57.21±1.211	42.71±1.11	1.61±0.79

Values are Mean±SD, n=3.

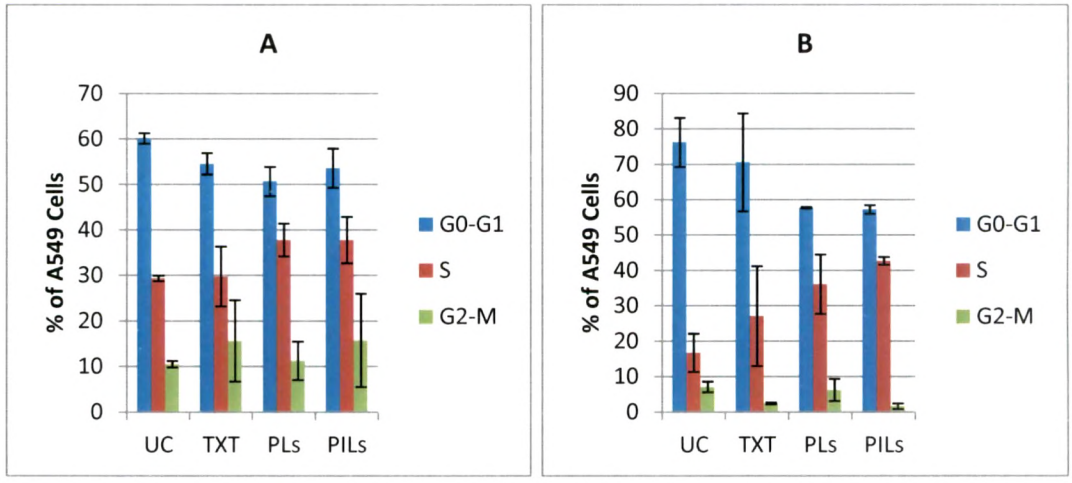

Figure 8.28. The % of A549 cells in G0-G1, S and G2-M phase after treatment with 2nM solution of Taxotere, PLs and PILs for a period of (A): 24hr and (B): 48hr

Table 8.8. The % of B16F10 cells in G0-G1, S and G2-M phase after treatment with 2nM solution of Taxotere, PLs and PILs for a period of 24hr and 48hr.

Drug	After 24hr treatment			After 48hr treatment		
	G0-G1	S	G2-M	G0-G1	S	G2-M
UC	63.54±12.7	24.46±15.5	11.99±2.9	76.26±10.95	17.04±9.3	6.69±1.5
TXT 2nM	63.71±5.7	19.77±11.6	16.51±6.2	72.92±6.55	20.6±4.1	6.48±2.3
PLs 2nM	60.75±8.3	28.74±7.4	10.5±1	74.34±8.8	17.6±5.4	8.05±3.3
PILs 2nM	60.92±10.6	28.34±8.7	10.72±3.1	74.20±8.1	17.1±6.8	7.9±1.3

Values are Mean±SD, n=3.

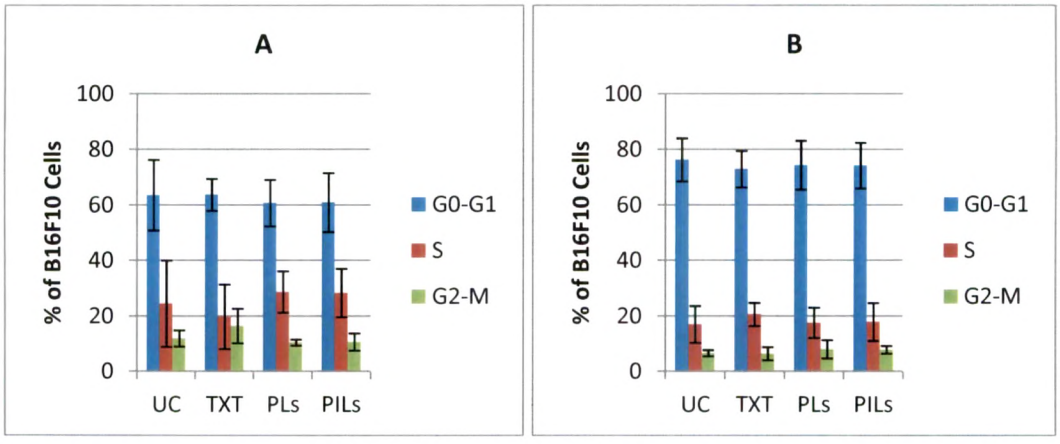

Figure 8.29. The % of B16F1o cells in G0-G1, S and G2-M phase after treatment with 2nM solution of Taxotere, PLs and PILs for a period of (A): 24hr and (B): 48hr

References

Baker AH, Edwards DR, Murphy G. Metalloproteinase inhibitors: biological actions and therapeutic opportunities. J. Cell Sci. 2002; 115:3719-3727.

Baskic D, Popovic S, Ristic P, Arsenijevic NN. Analysis of cycloheximide-induced apoptosis in human leukocytes: Fluorescence microscopy using annexin V/propidium iodide versus acridin orange/ethidium bromide. Cell Biol. Int. 2006; 30:924-932.

Bjornland K, Winberg JO, Odegaard OT, Hovig E, Loennechen T, Aasen AO, Fodstad O, Maelandsmo GM. S100A4 involvement in metastasis: deregulation of matrix metalloproteinases and tissue inhibitors of matrix metalloproteinases in osteosarcoma cells transfected with an anti-S100A4 ribozyme. Cancer Res. 1999; 59:4702-4708.

Bode W, Fernandez-Catalan C, Grams F, Gomis-Ruth FX, Nagase H, Tschesche H, Maskos K. Insights into MMP-TIMP interactions. Ann. NY Acad. Sci. 1999; 878:73-91.

Bode W, Maskos K. Structural basis of the matrix metalloproteinases and their physiological inhibitors, the tissue inhibitors of metalloproteinases. Biol. Chem. 2003; 384:863-872.

Bornique B, Lamarie A. Docetaxel (Taxotere®) is Not Metabolised by Recombinant Human CYP1B1 *In vitro*, but Acts as an Effector of This Isozyme. Drug Metab. Dispos. Vol. 30, No. 11, 2002, pp. 1149-1152.

Brew K, Dinakarpandian D, Nagase H. Tissue inhibitors of metalloproteinases: evolution, structure and function. Biochim. Biophys. Acta 2000; 1477:267-283.

Chin JR, Werb Z. Matrix metalloproteinases regulate morphogenesis, migration and remodeling of epithelium, tongue skeletal muscle and cartilage in the mandibular arch. Development 1997; 124:1519-1530.

Czejka M, Greil R, Ulsperger E, Schnait H, Kienesberger K, Brumnik T, Farkouh A, Schierholz J. Evidence for the conversion of docetaxel into 7-Epidocetaxel in patients receiving conventional chemotherapy with Taxotere. International J. Clin. Pharmacol. Ther. 2010; 48(7):483-484.

Egeblad M, Werb Z. New functions for the matrix metalloproteinases in cancer progression. Nat. Rev. Cancer 2002; 2(3):161-74.

Ellis LM. The Role of Neuropilins in Cancer. Mol. Cancer Ther. 2006; 5:1099-1107.

Etienne-Manneville S, Hall A. Rho GTPases in cell biology. Nature 2002; 420(6916):629-35.

Feng SS, Mei L, Anitha P, Gan CW, Zhou WY. Poly(lactide)-vitamin E derivative montmorillonite nanoparticle formulations for the oral delivery of Docetaxel. Biomaterials 2009; 30:3297-306.

Fernandez-Resa P, Mira E, Quesada AR. Enhanced detection of casein zymography of matrix metalloproteinases. Anal. Biochem. 1995; 224:434-435.

Friedl P, Wolf K. Tumour-cell invasion and migration: diversity and escape mechanisms. Nat. Rev. Cancer 2003; 3(5):362-74.

Goel PN, Gude RP. Unravelling the Antimetastatic Potential of Pentoxifylline, A Methylxanthine Derivative in Human MDA-MB-231 Breast Cancer Cells. Mol. Cell Biochem. 2011, 358:141-51.

Grant DS, Williams TL, Zahaczewsky M, Dicker AP. Comparison of antiangiogenic activities using paclitaxel (taxol) and docetaxel (taxotere). Int. J. Cancer. 2003; 104(1):121-9.

Grest GS, Cohen MH. Liquid-glass transition: Dependence of the glass transition on heating and cooling rates. Phys. Rev. B 21, 4113-4117 (1980)

Guo CB, Wang S, Deng C, Zhang DL, Wang FL, Jin XQ. Relationship between matrix metalloproteinase 2 and lung cancer progression. Mol. Diagn. Ther. 2007;11(3):183-92.

Hawkes SP, Li H, Taniguchi GT. Zymography and reverse zymography for detecting MMPs, and TIMPs, 2001, p.399-410. In. Clark I (Ed.), Matrix Metalloproteinases Protocols. Humana Press, Totowa, NJ.

Heussen C, Dowdle EB. Electrophoretic analysis of plasminogen activators in polyacrylamide gels containing sodium dodecyl sulfate and copolymerized substrates. Anal. Biochem. 1980; 102:196-202.

Hong TM, Chen YL, Wu YY, Yuan A, Chao YC, Chung YC, Wu MH, Yang SC, Pan SH, Shih JY, Chan WK, Yang PC. Targeting neuropilin 1 as an antitumor strategy in lung cancer. Clin. Cancer Res. 2007; 13:4759-4768.

Hu B, Guo P, Bar-Joseph I, Imanishi Y, Jarzynka MJ, Bogler O, Mikkelsen T, Hirose T, Nishikawa R, Cheng SY. Neuropilin-1 promotes human glioma progression through potentiating the activity of the hgf/sf autocrine pathway. Oncogene 2007; 26(38):5577-5586.

Kanzawa T, Kondo Y, Ito H, Kondo S, Germano I. Induction of Autophagic Cell Death in Malignant Glioma Cells by Arsenic Trioxide. Cancer Res. 2003; 63:2103-2108.

Kessenbrock K, Plaks V, Werb Z. Matrix metalloproteinases: regulators of the tumor microenvironment. Cell 2010; 2;141(1):52-67.

Kleiner DE, Stetler-Stevenson WG. Quantitative zymography: detection of picogram quantities of gelatinases. Anal. Biochem. 1994; 218:325-329.

Kogashiwa Y, Sakurai H, Kimura T, Kohno N. Docetaxel suppresses invasiveness of head and neck cancer cells *in vitro*. Cancer Sci. 2010; 101(6):1382-6.

Konttinen YT, Ainola M, Valleala H, Ma J, Ida H, Mandelin J, Kinne RW, Santavirta S et al. Analysis of 16 different matrix metalloproteinases (MMP-1 to MMP-20) in the synovial membrane: different profiles in trauma and rheumatoid arthritis. Ann. Rheum. Dis. 1999; 58:691-697.

Koziara JM, Lockman PR, Allen DD, Mumper RJ. Paclitaxel nanoparticles for the potential treatment of brain tumor. J. Control. Release 2004; 99:259-269.

Leber TM, Balkwill FR. Zymography: a single-step staining method for quantitation of proteolytic activity on substrate gels. Anal. Biochem. 1997; 249:24-28.

Lee HS, Seo EY, Kang NE, Kim WK. [6]-Gingerol inhibits metastasis of MDA-MB-231 human breast cancer cells. J. Nutr. Biochem. 2008; 19:313-319.

Lee JW, Thomas LC, Schmidt SJ. Effects of heating conditions on the glass transition parameters of amorphous sucrose produced by melt-quenching. J. Agric. Food. Chem. 2011; 59(7):3311-9.

Matsushita A, Gtze T, Korc M. Hepatocyte growth factor-mediated cell invasion in pancreatic cancer cells is dependent on neuropilin-1. Cancer Res. 2007; 67 (21):10309-10316.

Montero A, Fossella F, Hortobagyi G, Valero V. Docetaxel for treatment of solid tumours: a systematic review of clinical data. Lancet Oncol. 2005; 6:229-239.

Murtagh J, Lu H, Schwartz EL. Taxotere-induced inhibition of human endothelial cell migration is a result of heat shock protein 90 degradation. Cancer Res. 2006; 66(16):8192-9.

Nikkola J, Vihinen P, Vuoristo MS, Kellokumpu-Lehtinen P, Kähäri VM, Pyrhönen S. High serum levels of matrix metalloproteinase-9 and matrix metalloproteinase-1 are associated with rapid progression in patients with metastatic melanoma. Clin. Cancer Res. 2005; 15; 11(14):5158-66.

Ochiumi T, Kitadai Y, Tanaka S, Akagi M, Yoshihara M, Chayama K. Neuropilin-1 is involved in regulation of apoptosis and migration of human colon cancer. Int. J. Oncol. 2006; 29(1):105-16.

Oliver GW, Leferson JD, Stetler-Stevenson WG, Kleiner DE. Quantitative reverse zymography: analysis of picogram amounts of metalloproteinase inhibitors using gelatinase A and B reverse zymograms. Anal. Biochem. 1997; 244:161-166.

Pichot CS, Hartig SM, Xia L, Arvanitis C, Monisvais D, Lee FY, Frost JA, Corey SJ. Dasatinib synergizes with doxorubicin to block growth, migration, and invasion of breast cancer cells. Br. J. Cancer 2009; 101:38-47.

Pilcher BK, Wang M, Qin XJ, Parks WC, Senior RM, Welgus HG. Role of matrix metalloproteinases and their inhibition in cutaneous wound healing and allergic contact hypersensitivity. Ann. NY Acad. Sci. 1999; 878:12-24.

Polette M, Nawrocki-Raby B, Gilles C, Clavel C, Birembaut P. Tumour invasion and matrix metalloproteinases. Crit. Rev. Oncol. Hematol. 2004;49(3):179-86.

Pollock S, Antrobus R, Newton L, Kampa B, Rossa J, Latham S, Nichita NB, Dwek RA, Zitzmann N. Uptake and trafficking of liposomes to the endoplasmic reticulum. FASEB J. 2010; 24(6):1866-78.

Polo ML, Arnoni MV, Riggio M, Wargon V, Lanari C, Novaro V. Responsiveness to PI3K and MEK inhibitors in breast cancer. Use of a 3D culture system to study pathways related to hormone independence in mice. PLoS One 2010; 5:e10786

Pöschl E, Schlötzer-Schrehardt U, Brachvogel B, Saito K, Ninomiya Y, Mayer U. Collagen IV is essential for basement membrane stability but dispensable for initiation of its assembly during early development. Development 2004;131(7):1619-28.

Prud'homme GJ, Glinka Y. Neuropilins are multifunctional coreceptors involved in tumor initiation, growth, metastasis and immunity. Oncotarget, Advanced publications 2012; 1-19.

Renvoize C, Biola A, Pallardy M, Breard J. Apoptosis: identification of dying cells. Cell Biol. Toxicol. 1998; 14:111-120

Ribble D, Goldstein NB, Norris DA, Shellman YG. A simple technique for quantifying apoptosis in 96-well plates. BMC Biotechnol. 2005; 5:12

Salma J, McDermott JC. Suppression of a MEF2-KLF6 Survival Pathway by PKA Signaling Promotes Apoptosis in Embryonic Hippocampal Neurons. J. Neurosci. 2012; 32(8):2790-2803.

Serpe L, Catalano MG, Cavalli R, Ugazio E, Bosco O, Canaparo R, Muntoni E, Frairia R, Gasco MR, Eandi M, Zara GP. Cytotoxicity of anticancer drugs incorporated in solid lipid nanoparticles on HT-29 colorectal cancer cell line. Eur. J. Pharm. Biopharm. 2004; 58:673-680.

Sharma A, Sharma US, Straubinger RM. Paclitaxel-liposomes for intracavity therapy of intraperitoneal P388 leukemia. Cancer Lett. 1996; 107:265-272.

Song H, Zhang J, Han Z, Zhang X, Li Z, Zhang L, Fu M, Lin C, Ma J. Pharmacokinetic and cytotoxic studies of pegylated liposomal daunorubicin. Cancer Chemother. Pharmacol. 2006; 57:591-598.

Springman EB, Angleton EL, Birkedal-Hansen H, Van Wart HE. Multiple modes of activation of latent human fibroblast collagenase: evidence for the role of a Cys73 active-site zinc complex in latency and a "cysteine switch" mechanism for activation. Proc. Natl. Acad. Sci. USA 1990; 87:364-368.

Thomas LC. Use of multi heating rate DSC and modulated temperature DSC to detect and analyse temperature and time dependent transitions in materials. Reprinted from American Laboratory January 2001

Twentyman PR, Luscombe M. A study of some variables in a tetrazolium dye (MTT) based assay for cell growth and chemosensitivity. Br. J. Cancer 1987; 56:279-285.

Wang S, Liu Q, Zhang Y, Liu K, Yu P, Liu K, Luan J, Duan H, Lu Z, Wang F, Wu E, Yagasaki K, Zhang G. Suppression of growth, migration and invasion of highly-metastatic human breast cancer cells by berbamine and its molecular mechanisms of action. Mol. Cancer 2009; 8:81.

Watanabe T, Noritake J, Kaibuchi K. Regulation of microtubules in cell migration. Trends. Cell Biol. 2005; 15(2):76-83.

Woessner JF. Quantification of matrix metalloproteinases in tissue samples. Methods Enzymol. 1995; 248:510-528.

Wong HL, Bendayan R, Rauth AM, Xue HY, Babakhanian K, Wu XY. A mechanistic study of enhanced doxorubicin uptake and retention in multidrug resistant breast cancer cells using a polymer-lipid hybrid nanoparticle (PLN) system. J. Pharmacol. Exp. Ther. 2006; 317:1372-1381.

Wong HL, Bendayan R, Rauth AM, Li Y, Wu XY. Chemotherapy with anticancer drugs encapsulated in solid lipid nanoparticles. Adv. Drug Deliv. Rev. 2007; 59:491-504.

Xie F, Yao N, Qin Y, Zhang Q, Chen H, Yuan M, Tang J, Li X, Fan W, Zhang Q, Wu Y, Hai L, He Q. Investigation of glucose-modified liposomes using polyethylene glycols with different chain lengths as the linkers for brain targeting. Int. J. Nanomedicine 2012; 7:163-175.

Yanasarn N, Sloat BR, Cui Z. Nanoparticles engineered from lecithin-in-water emulsions as a potential delivery system for docetaxel. Int. J. Pharm. 2009; 379:174-180.

Yang T, Cui FD, Choi MK, Choc JW, Chung SJ, Shimb CK, Kimb DD. Enhanced solubility and stability of PEGylated liposomal paclitaxel: *In vitro* and *in vivo* evaluation. Int. J. Pharm. 2007; 338:317-326.

Yu WH, Woessner Jr JF. Heparin-enhanced zymographic detection of matrilysin and collagenases. Anal. Biochem. 2001; 293:38-42.

Zhang C, Ping Q, Zhang H. Self-assembly and characterization of paclitaxel-loaded N-octyl-O-sulfate chitosan micellar system. Colloids Surf. 2004; 39:69-75.